

# NMR effective Hamiltonian engineering and decoupling

by

A.A. Bonke

to obtain the degrees of Bachelor of Science in Applied Physics and Bachelor of Science in Applied  
Mathematics  
at the Delft University of Technology,  
to be defended publicly on Tuesday June 28, 2022 at 14:00.

Student number: 5134080  
Project duration: March, 2022 – June, 2022  
Supervisors: Dr. J.L.A. Dubbeldam  
Dr. D. Kwiatkowski  
Dr. T.H. Taminiau  
Thesis committee: Dr. N.V. Budko  
Dr. J.L.A. Dubbeldam  
Dr. T. van der Sar  
Dr. T.H. Taminiau

An electronic version of this thesis is available at <http://repository.tudelft.nl/>.

We introduce a method of designing NMR pulse sequences, with a specific focus toward complete decoupling of carbon-13 spin qubits coupled to a nitrogen-vacancy (NV) center in diamond. Using Average Hamiltonian Theory, we calculate different intermediate Hamiltonians corresponding to different rotations implemented by NMR pulses. Two novel pulse sequences are obtained containing 24 and 12 evolution periods respectively. Assuming ideal and instantaneous pulses, performance for both sequences is better than the WAHUHA + echo sequence for total evolution times of less than 5 ms and comparable for greater evolution times. Analysis of sensitivity points toward non-robustness for angle errors in the applied pulses when the direction of pulses is not taken into account, however this can be corrected for using chirality sums. Suggestions for further research include the study of non-globally applied pulses and application of the design method to non-zero effective Hamiltonians.

# Contents

1	Introduction	1
2	The mathematical formalism of quantum mechanics	3
2.1	Bra-ket notation	3
2.2	Operators and unitaries	3
2.3	Time evolution of quantum states	4
2.4	The density matrix	4
2.5	The rotation operator	7
2.6	Fidelity	7
3	NMR control of qubits	9
3.1	Quantum states and the Bloch sphere	9
3.2	Larmor precession and the Zeeman Hamiltonian	10
3.3	Rabi oscillations and resonance	11
3.4	The rotating frame	13
4	The nitrogen vacancy center in diamond	15
4.1	The crystal structure of diamond	15
4.2	NV-center	16
4.3	Dipolar couplings	17
5	Designing the pulse sequence	19
5.1	Average Hamiltonian Theory	19
5.2	Rotational symmetries and orientations	20
5.3	Linear Programming in NMR pulse design	21
5.4	Symmetry considerations	22
5.5	Internuclear interactions	24
6	Results	27
6.1	Pulse sequence 1: 24 orientations	27
6.2	Pulse sequence 2: 12 orientations	31
7	Discussion	35
7.1	Consecutiveness of pulses	35
7.2	Heterogeneous pulse combinations	35
7.3	Non-ideality of pulses	36
7.4	Tilted axis pulses	36
7.5	Coupling strengths	36
8	Conclusion	39
A	Tables of couplings	41
B	Analytical result	43



# 1

## Introduction

In 2021, researchers at QuTech demonstrated a discrete time crystal [1]. This novel state of matter, which oscillates between two discrete states, was first theoretically proposed in 2012 [2]. 9 qubits in a diamond/nitrogen vacancy center system were used to form the crystal, which showed extremely long lifetimes of 8 seconds. Furthermore, formation of the DTC phase showed robustness to initial conditions. This experiment has far-reaching consequences, including a possible approach to quantum memory.

Quantum information processing as a field is dependent on good control, readout and retention capabilities for quantum information. Practical implementations of quantum technologies such as the example above require comprehensive controllability of system dynamics. Furthermore, the system needs to be sufficiently protected from decoherence. One way of accomplishing these goals is by effective Hamiltonian engineering. This technique often relies on Average Hamiltonian Theory, which is a mathematical framework for transforming a time-dependent system Hamiltonian to a time-independent effective Hamiltonian. The system state is then affected as if the system were evolving according to the effective Hamiltonian over the total evolution period.

For qubits in the form of nuclear spins, such effective Hamiltonians can be tuned to desired specifications using magnetic resonance pulses (NMR). Through the application of static and rotating magnetic fields the Hamiltonian of a system can be essentially rotated over an axis. A clever scheme of applied pulses can then cancel out certain interactions or recouple others, providing an effective Hamiltonian which is adapted to the desired system dynamics.

In this thesis, this technique of NMR pulse engineering will be applied to the complete decoupling of carbon-13 spins in diamond coupled to a nitrogen-vacancy center. Using techniques from linear algebra and optimization, a formalism will be set up for the design of decoupling pulse sequences. This formalism will be used to design two pulse sequences (A-24 and A-12) and the performance of these pulse sequences will be graded and compared.



# 2

## The mathematical formalism of quantum mechanics

In this chapter we will briefly provide a selection of techniques from linear algebra which will be used throughout the thesis, in the context of physically relevant quantities. The reader is assumed to be familiar with quantum mechanics.

### 2.1. Bra-ket notation

When representing quantum states and operators, it is convenient to use the bra-ket notation [3]:

$$\langle \psi |, | \psi \rangle, \quad (2.1)$$

where the ‘bra’ corresponding to the left angle bracket and the vertical bar denotes a linear mapping from a (complex) vector in a Hilbert space to a (complex) scalar and the ‘ket’ corresponding to the vertical bar and the right angle bracket denotes a vector in a Hilbert space. Note that this is different from an operator: an operator acting on a ket yields another ket, while a bra acting on a ket yields a scalar. Operators will be discussed in the next section.

Bras and kets can be used to denote inner products between states:

$$\langle \psi | \phi \rangle = \int \psi^* \phi. \quad (2.2)$$

Here, the bra is understood to be a covector corresponding to a state vector in Hilbert space. Inner products between quantum states signify ‘overlap’ between them. The squared absolute value of the inner product between two states  $|\langle \psi | \phi \rangle|^2$  is a probability equal to the chance of finding state  $|\psi\rangle$  in state  $|\phi\rangle$ .

This bra-ket notation is extremely useful, because it is a bridge between wavefunctions and vectors, both used as tools in quantum mechanics for denoting quantum states. In this thesis, the Hilbert space that will be used is  $\mathbb{C}^n$  equipped with the Hermitian inner product. Kets then represent column vectors, operators are matrices and it is natural to see bras as row vectors so that an inner product can be carried out using standard matrix/vector multiplication. Formally, a bra can be considered as the Hermitian transpose of a ket.

### 2.2. Operators and unitaries

Operators transform one quantum state into another. They lie at the center of the mathematical formulation of quantum mechanics. An operator which is acting on a ket is placed on the left side of that ket:

$$\hat{A} | \psi \rangle, \quad (2.3)$$

and is represented by an  $n \times n$  matrix, where  $n$  is the dimension of the Hilbert space. Operators which represent physically measurable quantities are called observables. These operators correspond to Hermitian matrices as these are guaranteed to have real eigenvalues: physically observable quantities have real numbered values.

Using observables, we can gain information about the quantum system. Quantum mechanics is a probabilistic theory: information about a system may not have one specific value, but rather a distribution of values associated with it. If we want to connect quantum systems to real-world measurable quantities, it makes sense to use some sort of statistical metric. This is why expectation values are used to gain information about a certain system. Expectation values for observables are defined analogously to inner products:

$$\langle \hat{A} \rangle = \int \psi^* \hat{A} \psi = \langle \psi | \hat{A} | \psi \rangle. \quad (2.4)$$

### 2.3. Time evolution of quantum states

An essential operator in quantum mechanics is the Hamiltonian. This operator, denoted by  $\hat{H}$  or  $H$ , corresponds to the total energy of a system, i.e. the sum of potential and kinetic energy. A system evolves freely according to this Hamiltonian.

The time-dependent Schrödinger equation, which governs the dynamics of quantum systems, assumes the following form in bra-ket notation:

$$i\hbar \frac{\partial}{\partial t} |\psi(t)\rangle = \hat{H} |\psi(t)\rangle. \quad (2.5)$$

If the Hamiltonian  $\hat{H}$  is time-independent, the solution to the Schrödinger equation can be represented as:

$$|\psi(t)\rangle = e^{-i\hat{H}t/\hbar} |\psi(0)\rangle. \quad (2.6)$$

The exponential here is known as the time evolution operator and is denoted by  $\hat{U}(t)$ . Since  $\hat{H}$  is Hermitian, the matrix exponential above is a unitary operator:  $\hat{U}(t)^\dagger \hat{U}(t) = e^{i\hat{H}^\dagger t/\hbar} e^{-i\hat{H}t/\hbar} = I$  where  $I$  is the identity matrix.

### 2.4. The density matrix

Using bra-ket notation, we can easily denote superpositions of states:

$$|\psi\rangle = \frac{1}{\sqrt{2}} (|\uparrow\rangle + |\downarrow\rangle). \quad (2.7)$$

One problem with this notation, however, arises when we want to represent classical mixtures of states. Suppose, for example, we want to prepare particles in the  $|\uparrow\rangle$  state. However, the experimental setup which is used to prepare the particles is faulty, so that 95% of particles are prepared in the  $|\uparrow\rangle$  state and 5% of particles are prepared in the  $|\downarrow\rangle$  state. This is impossible to denote with standard bra-ket notation.

It is important to realize that the situation described above is something fundamentally different from equation 2.7: the superposition is a vector in Hilbert space, but the classical mixture of states is not. States which we can represent as a vector in Hilbert space are called pure states, and states for which this is not possible are called mixed. Since we cannot write mixed states using bra-ket notation we use a formalism known as the density matrix [4]. For a pure state  $|\psi\rangle$ , the density matrix is denoted by  $\rho$  and is defined as:

$$\rho = |\psi\rangle \langle \psi|. \quad (2.8)$$

In other words, the density matrix for a pure state, which can be represented as a ket, is defined as the outer product of that ket with itself. For a mixed state, the density matrix is defined as

$$\rho = \sum_j p_j \rho_j, \quad (2.9)$$

where the  $\rho_j$  are the density matrices for each of the pure states which constitute the mixed state and  $p_j$  denotes the classical probability assigned to each state respectively.

For example, the state produced by the faulty machinery described in a previous paragraph would have density matrix

$$\rho = 0.95 |\uparrow\rangle \langle \uparrow| + 0.05 |\downarrow\rangle \langle \downarrow| = \begin{pmatrix} 0.95 & 0 \\ 0 & 0.05 \end{pmatrix}, \quad (2.10)$$

where we chose the conventional basis  $|\uparrow\rangle = \begin{pmatrix} 1 \\ 0 \end{pmatrix}$ ,  $|\downarrow\rangle = \begin{pmatrix} 0 \\ 1 \end{pmatrix}$ . This is the basis that will be used in the rest of this thesis.

The density matrix as defined above has certain properties:

- $\rho$  is Hermitian. For a pure state:

$$\rho^\dagger = (|\psi\rangle\langle\psi|)^\dagger = \langle\psi|^\dagger|\psi\rangle^\dagger = |\psi\rangle\langle\psi| = \rho. \quad (2.11)$$

Hermiticity holds under linear combination, so the above property applies to mixed states as well.

- $\text{Tr}(\rho) = 1$ . For pure states we have

$$\text{Tr}(\rho) = \sum_n \langle n|\psi\rangle\langle\psi|n\rangle \quad (2.12)$$

$$\text{Tr}(\rho) = \sum_n |\langle\psi|n\rangle|^2 = 1, \quad (2.13)$$

where the equality to 1 follows from the normalisation of the quantum state. From linearity of the trace it follows that mixed states have  $\text{Tr}(\rho) = 1$  as well.

- For pure states,  $\rho^2 = \rho$ . Indeed this is obvious from bra-ket notation:

$$\rho^2 = |\psi\rangle\langle\psi|\psi\rangle\langle\psi| = |\psi\rangle\langle\psi| = \rho, \quad (2.14)$$

where we use normalization of the state. This is not the case for mixed states. Take for example the completely mixed state:

$$\rho = \frac{1}{2} \begin{pmatrix} 1 & 0 \\ 0 & 1 \end{pmatrix}, \quad (2.15)$$

for which the property clearly does not hold.

- $\text{Tr}(\rho^2) \leq 1$  where equality holds only for pure states.

$$\text{Tr}(\rho^2) = \sum_n \langle n|\sum_i \sum_j p_i p_j |\psi_i\rangle\langle\psi_i|\psi_j\rangle\langle\psi_j|n\rangle, \quad (2.16)$$

where again  $|n\rangle$  is an orthonormal basis for the Hilbert space. Using linearity

$$\text{Tr}(\rho^2) = \sum_n \sum_i \sum_j p_i p_j \langle n|\psi_i\rangle\langle\psi_i|\psi_j\rangle\langle\psi_j|n\rangle. \quad (2.17)$$

Rearranging bra-ket products (which are scalars):

$$\text{Tr}(\rho^2) = \sum_i \sum_j \sum_n p_i p_j \langle\psi_j|n\rangle\langle n|\psi_i\rangle\langle\psi_i|\psi_j\rangle. \quad (2.18)$$

Finally, taking out identity and assuming orthogonality of eigenstates:

$$\text{Tr}(\rho^2) = \sum_i p_i^2 |\langle\psi_i|\psi_i\rangle|^2 = \sum_i p_i^2 \leq \sum_i p_i = 1. \quad (2.19)$$

Strict inequality holds if and only if at least one of the  $p_i$  is smaller than 1, that is, if we have a mixed state. Only pure states then have  $\text{Tr}(\rho^2) = 1$  (indeed, for pure states  $\text{Tr}(\rho^2) = \text{Tr}(\rho) = 1$ ). We define the quantity  $\text{Tr}(\rho^2)$  to be the purity of the state.

- For an operator  $\hat{A}$ , the expectation value  $\langle\hat{A}\rangle$  can be obtained from the density matrix as  $\langle\hat{A}\rangle = \text{Tr}(\rho\hat{A})$ . Starting from an arbitrary (mixed) state:

$$\text{Tr}(\rho\hat{A}) = \sum_j p_j \text{Tr}(|\psi_j\rangle\langle\psi_j|\hat{A}), \quad (2.20)$$

where we used linearity of trace,

$$\text{Tr}(\rho\hat{A}) = \sum_j p_j \sum_n \langle n|\psi_j\rangle\langle\psi_j|\hat{A}|n\rangle, \quad (2.21)$$

where the  $|n\rangle$  are an orthonormal basis for our Hilbert space. The bra-ket products yield scalars which commute:

$$\text{Tr}(\rho\hat{A}) = \sum_j p_j \sum_n \langle\psi_j|\hat{A}|n\rangle\langle n|\psi_j\rangle, \quad (2.22)$$

finally the outer products of the basis vectors reduce to identity

$$\text{Tr}(\rho \hat{A}) = \sum_j p_j \langle \psi_j | \hat{A} | \psi_j \rangle, \quad (2.23)$$

and we are left with a convex combination of the expectation values of each of the component states with each state weighted by its respective classical probability.

- The density matrix of a two-level system can be written as a linear combination of identity and the Pauli matrices. We claim

$$\rho = \frac{1}{2}(I + r_x \sigma_x + r_y \sigma_y + r_z \sigma_z). \quad (2.24)$$

For an arbitrary 2 x 2 density matrix, we can use that  $\text{Tr}(\rho) = 1$  and that  $\rho$  is Hermitian to write

$$\rho = \begin{pmatrix} a & b^* \\ b & 1-a \end{pmatrix}, \quad (2.25)$$

where  $a$  is real because  $\rho$  is Hermitian, and  $b$  may be complex. Now,

$$\rho = \frac{1}{2}I + \begin{pmatrix} a - \frac{1}{2} & b^* \\ b & \frac{1}{2} - a \end{pmatrix}. \quad (2.26)$$

This can be readily decomposed into Pauli matrices:

$$\rho = \frac{1}{2}I + \Re(b) \begin{pmatrix} 0 & 1 \\ 1 & 0 \end{pmatrix} + \Im(b) \begin{pmatrix} 0 & -i \\ i & 0 \end{pmatrix} + (a - \frac{1}{2}) \begin{pmatrix} 1 & 0 \\ 0 & -1 \end{pmatrix}, \quad (2.27)$$

which is clearly equal to 2.24 with coefficients  $r_x = 2\Re(b)$ ,  $r_y = 2\Im(b)$ ,  $r_z = 2a - 1$ . Note that the coefficients we obtained are all real.

Now that we have proved equation 2.24 we can obtain the  $r_i$  in a more elegant way. We claim  $r_i = \text{Tr}(\rho \sigma_i)$  (which would be the expectation value of  $\sigma_i$ ). Starting from equation 2.24 we use the following properties of Pauli matrices:

- $\sigma_i \sigma_j = i \epsilon_{ijk} \sigma_k$ ,  $i \neq j$ ,  
where  $\epsilon_{ijk}$  is the Levi-Civita symbol.<sup>1</sup> This means the Pauli matrices are anticommutative (when not multiplied by themselves).
- $\sigma_i \sigma_i = I$ .
- $\text{Tr}(\sigma_i) = 0$ ,  $\text{Tr}(I) = 2$ .

These properties are easily verified and the respective proofs will be omitted. Now, when computing  $\text{Tr}(\rho \sigma_i)$  the 'cross terms' between different Pauli matrices and between Pauli matrices and identity vanish:

$$\text{Tr}(\rho \sigma_i) = \frac{1}{2} \text{Tr}(\sigma_i + r_x \sigma_x \sigma_i + r_y \sigma_y \sigma_i + r_z \sigma_z \sigma_i) = \frac{1}{2} \text{Tr}(r_i \sigma_i \sigma_i) = r_i, \quad (2.28)$$

as claimed. In fact, this principle generalizes to all Hermitian matrices when including an extra degree of freedom as the trace need not be 1:

$$A = \frac{1}{2}(c_0 \sigma_0 + c_x \sigma_x + c_y \sigma_y + c_z \sigma_z), \quad (2.29)$$

where we denoted the identity matrix by  $\sigma_0$ . Like in 2.28 we can obtain the coefficients  $c_i$  by tracing:

$$c_i = \text{Tr}(A \sigma_i). \quad (2.30)$$

This is called a Pauli projection and the corresponding  $c_i$  are called Pauli coefficients. [5] The result also generalizes to  $2^n \times 2^n$  Hermitian matrices using tensor products of the Pauli matrices:

$$S_{i,j,k,\dots} \equiv \sigma_i \otimes \sigma_j \otimes \sigma_k \otimes \dots \quad (2.31)$$

The resulting projection will contain  $4^n$  coefficients. We will denote the Pauli projection by:

$$\mathcal{P}(A) \equiv \mathbf{c}_A. \quad (2.32)$$

This projection is linear and provides a 'natural' basis of representing Hermitian matrices. This projection will become very important later on for optimization.

<sup>1</sup> $\epsilon_{ijk}$  is equal to +1 when the indices are in the 'right' order (x, y, z) or cyclic permutations thereof {(y, z, x), (z, x, y)} and is equal to -1 otherwise.

## 2.5. The rotation operator

At the basis of NMR control, lies the application of rotations to quantum states. In particular, for a two-level spin- $\frac{1}{2}$  system which is rotated around the x-, y-, or z-axis, the rotation operator assumes the form [6]

$$R_j(\theta) = e^{-i\theta I_j}, \quad (2.33)$$

where  $\theta$  is the rotation angle and  $j$  is the index indicating the axis of rotation.  $I_j$  indicates the spin matrix corresponding to the rotation axis defined as  $I_j = \frac{1}{2}\sigma_j$ .<sup>2</sup> The rotation operator is unitary:

$$R_j(\theta)^\dagger R_j(\theta) = e^{i\theta I_j^\dagger} e^{-i\theta I_j} = I. \quad (2.34)$$

Alternatively, we can look at the series expansion of the exponential to obtain

$$R_j(\theta) = e^{-i\frac{\theta}{2}\sigma_j} \quad (2.35)$$

$$R_j(\theta) = I - i\frac{\theta}{2}\sigma_j - \frac{1}{2!}\left[\frac{\theta}{2}\right]^2 I + i\frac{1}{3!}\left[\frac{\theta}{2}\right]^3 \sigma_j \dots \quad (2.36)$$

using  $\sigma_j^2 = I$ . We recognize the series expansion of sine and cosine here:

$$R_j(\theta) = \cos\frac{\theta}{2}I - i\sin\frac{\theta}{2}\sigma_j. \quad (2.37)$$

To be precise, this would define a left-handed coordinate system because of the negative exponent in the rotation operator (this is conventional). However, it is also conventional to use a right-handed coordinate system, so we will show a right-handed system when necessary, keeping in mind that rotations are strictly speaking in the ‘wrong’ direction.

## 2.6. Fidelity

In later sections, when quantifying how much alike two quantum states are, it makes sense to define some metric for this purpose. One such metric is fidelity. We use the definition of fidelity as given by Nielsen and Chuang [8]. The definition given below does not define an actual metric on the space of density matrices according to the mathematical definition, but it provides a useful statistic for comparing quantum states:

$$F(\rho, \sigma) = \text{Tr} \sqrt{\sqrt{\rho}\sigma\sqrt{\rho}}, \quad (2.38)$$

where  $\rho$  and  $\sigma$  are two density matrices. Notice that the square root of a matrix appears here:  $\sqrt{\rho}$  is a matrix such that  $\sqrt{\rho}^2 = \rho$ . But if  $\sqrt{\rho}$  satisfies  $\sqrt{\rho}^2 = \rho$ , so does  $-\sqrt{\rho}$ . Therefore, by convention, we choose  $\sqrt{\rho}$  to have positive eigenvalues. Such a matrix can be calculated using spectral theory. Fidelity has a nice and intuitive property with regard to the values which it takes on:

$$0 \leq F(\rho, \sigma) \leq 1, \quad (2.39)$$

where a higher fidelity signifies higher resemblance between the two quantum states. Remember that for pure states, we have  $\rho^2 = \rho$ , so that pure state density matrices are their own matrix square root. Suppose we want to calculate  $F(\rho, \sigma)$  where  $\rho = |\psi\rangle\langle\psi|$  and  $\sigma = |\phi\rangle\langle\phi|$  are both pure states:

$$F(\rho, \sigma) = \text{Tr} \sqrt{|\psi\rangle\langle\psi|\langle\psi|\phi\rangle\langle\phi|\psi\rangle\langle\psi|} \quad (2.40)$$

$$F(\rho, \sigma) = \text{Tr} \sqrt{|\langle\psi|\phi\rangle|^2 |\psi\rangle\langle\psi|} \quad (2.41)$$

$$F(\rho, \sigma) = |\langle\psi|\phi\rangle| |\text{Tr}(\rho)| = |\langle\psi|\phi\rangle|. \quad (2.42)$$

In the last step we took the constant bra-ket product outside of the square root and trace, and recognized the (pure) density matrix  $\rho$  which is its own square root and has unit trace. For pure states then, fidelity is defined as the absolute value of the inner product between the two quantum states. This means fidelity is intimately connected with overlap between states. One more important property is that  $F(\rho, \sigma)$  is symmetric in  $\rho, \sigma$ . For the proof we refer to Nielsen and Chuang [8].

<sup>2</sup>The spin operator  $I_z$  is often defined to include a factor of  $\hbar$ , but we follow Oliveira et al. [7] here in designating  $I_z$  to be a dimensionless spin operator. One reason for this is that the factor  $\hbar$  is cancelled out when calculating a unitary propagator, so omitting it altogether (so also the division by  $\hbar$  in the exponent of the unitary propagator) tidies up the equations.



# 3

## NMR control of qubits

In this chapter, we describe a two-level quantum system (a qubit) in the form of a nuclear spin. We introduce the control dynamics of this system under the application of static and dynamic magnetic fields.

### 3.1. Quantum states and the Bloch sphere

In the previous chapter we introduced a representation of the quantum state as a density matrix. Although some information about the state can be readily distilled from the structure of the matrix itself, a more comprehensive visual intuition is still lacking. This motivates the use of the Bloch sphere for the representation of quantum states of a two-level system.

Recall equation 2.24. We used properties of the density matrix to extract three real coefficients which provide a complete description of the state. We can view these three coefficients as constituting a vector in  $\mathbb{R}^3$ . We call this the Bloch vector. We claim that such a vector lies on or within the unit sphere. Indeed, if we look at the purity of  $\rho$ :

$$\text{Tr}(\rho^2) = \frac{1}{4} \text{Tr}((I + r_x \sigma_x + r_y \sigma_y + r_z \sigma_z)^2), \quad (3.1)$$

where, as in equation 2.28, the ‘cross terms’ cancel out, leaving

$$\text{Tr}(\rho^2) = \frac{1}{2} (1 + r_x^2 + r_y^2 + r_z^2) = \frac{1}{2} (1 + |r|^2), \quad (3.2)$$

where we denoted with  $|r|^2$  the length of our Bloch vector and used the coefficients obtained in the previous chapter. It was shown before that  $\text{Tr}(\rho^2) \leq 1$  such that

$$|r|^2 \leq 1, \quad (3.3)$$

with equality holding only for pure states. It readily follows that pure states have Bloch vector of length 1, whereas mixed states have Bloch vectors of length smaller than 1. The unit sphere in  $\mathbb{R}^3$  which contains these vectors is called the Bloch sphere in this context. Pure and mixed states will then correspond to points on the surface and in the interior of this sphere respectively. Some examples of density matrices with their corresponding Bloch vectors are given below:

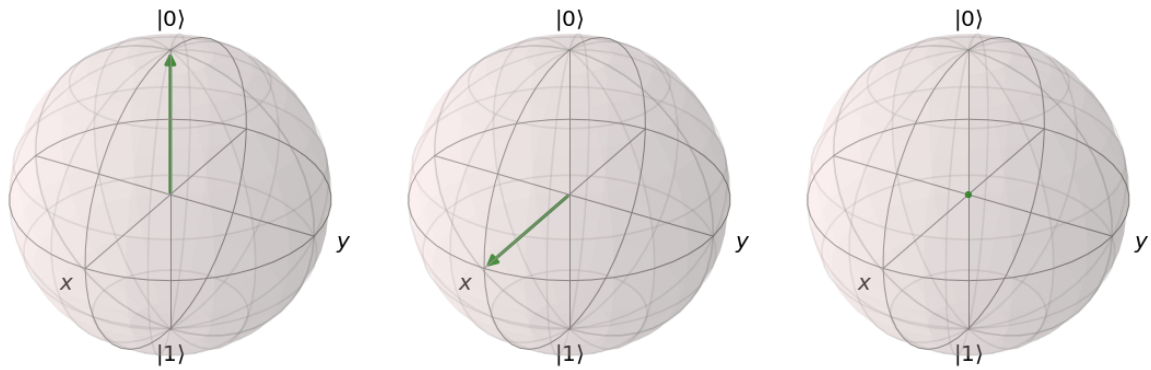


Figure 3.1:

$$\rho = \begin{pmatrix} 1 & 0 \\ 0 & 0 \end{pmatrix}$$

|↑⟩ state.

Figure 3.2:

$$\rho = \frac{1}{2} \begin{pmatrix} 1 & 1 \\ 1 & 1 \end{pmatrix}$$

|+x⟩ state.

Figure 3.3:

$$\rho = \frac{1}{2} \begin{pmatrix} 1 & 0 \\ 0 & 1 \end{pmatrix}$$

Completely mixed state.

The Bloch sphere is especially useful when describing rotations and evolutions of quantum states.

### 3.2. Larmor precession and the Zeeman Hamiltonian

Classical objects can have angular momentum in one of two ways: either by rotating around their own axis, or around another axis. Quantum mechanical objects can have angular momentum in the second sense as well: an electron bound to an atom is an example. But quantum objects cannot rotate around their own axis as they do not have well-defined dimensions in the way that, for example, a tennis ball can have. There is, however, a form of angular momentum in quantum mechanics that is analogous to a classical object spinning about its own axis. This angular momentum, which is an intrinsic property of a particle, is called spin for this reason. It is quantized, meaning it can take on only discrete values.

If a nucleus has a nonzero spin, it constitutes a magnetic dipole moment. Placing the dipole in a static magnetic field will cause a splitting in the energy levels of the nuclei according to the orientation of the spin with respect to the magnetic field. This is called the Zeeman effect. Without loss of generality, it is conventional to choose the axes such that the static magnetic field is pointing in the positive z-direction. For a classical magnetic moment, torque is exerted on the magnetic moment by the static field, which results in a precession of the magnetic moment around the direction of the field. This motion is called Larmor precession. This effect is completely analogous to a spinning top, where the magnetic moment is actual angular momentum instead and the field exerting torque is a gravitational field.

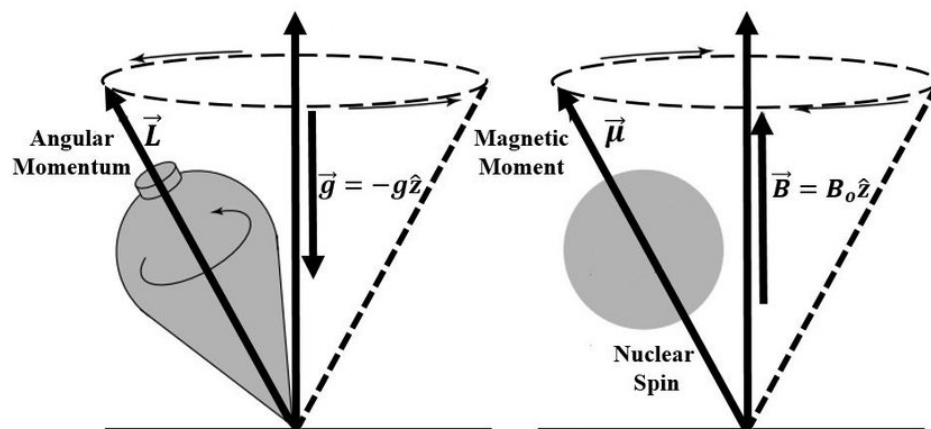


Figure 3.4: A magnetic moment precessing in a static magnetic field, analogous to a spinning top in a gravitational field. Sourced from [9].

The Hamiltonian which is introduced due to the orientation of a nuclear magnetic moment  $\mu$  with respect

to the field  $\mathbf{B}_0$  is [10]

$$\hat{H}_0 = -\hat{\boldsymbol{\mu}} \cdot \mathbf{B}_0 = -\hat{\mu}_z B_0 = -\gamma_n \hbar B_0 \hat{I}_z, \quad (3.4)$$

where we introduced the gyromagnetic ratio of the nucleus  $\gamma_n$  and the spin operator  $I_z = \frac{1}{2}\sigma_z$ . The factor  $\gamma_n B_0$  is the frequency at which the magnetic moment precesses and is denoted by  $\omega_L$ . This can be derived from the dynamic equations of motion [10]. The eigenstates of this Hamiltonian then correspond to the eigenstates of  $I_z$ . This Hamiltonian provides a more mathematical insight into Larmor precession. The spin operator  $I_z$  commutes with the Hamiltonian (of course, any operator commutes with itself) but its counterparts  $I_x$  and  $I_y$  do not. Therefore, the expectation of  $I_z$  will remain constant under evolution according to the Hamiltonian, but the expectation values of  $I_x$  and  $I_y$  will oscillate in time. [11] This is what constitutes Larmor precession. The minus sign in front of the Hamiltonian points out that spins aligned parallel to the field have lower energy than spins aligned in an antiparallel manner.

### 3.3. Rabi oscillations and resonance

In the previous section, we described the interaction of a nucleus carrying spin with a static magnetic field. Now we will look at oscillating magnetic fields and how these fields can rotate the spins, provided they are applied at the right frequency. The derivation below does not provide the general solution for a two-level system transitioning between arbitrary states, but instead aims to illustrate the general principle of rotation using oscillating magnetic fields.

The required oscillation frequency for the magnetic field turns out to be the Larmor frequency, as we will show. The Larmor frequency for nuclear spins subjected to commonly used field strengths is in the order of MHz, which is the radiofrequency range [7]. For this reason, the Hamiltonian corresponding to the oscillating field is commonly denoted as  $\hat{H}_{rf}$ . Let's now define a general time dependent field  $\mathbf{B}_1(t)$  and derive the resulting Hamiltonian in the same manner:

$$\hat{H}_{rf} = -\hat{\boldsymbol{\mu}} \cdot \mathbf{B}_1(t) = -\gamma_n \hbar \mathbf{B}_1(t) \cdot \hat{\mathbf{I}}, \quad (3.5)$$

where  $\mathbf{I}$  contains the three spin operators. The magnitude of the RF field is much smaller than that of the static field, typically by a factor of  $10^4$  [7]. Therefore we can treat  $\hat{H}_{rf}$  as a perturbation to  $\hat{H}_0$  and use time-dependent perturbation theory to work out the dynamics of this system. We follow the approach of Griffiths and Schroeter [11].

We start out with the two eigenstates of the unperturbed Hamiltonian (these are the eigenstates of  $\hat{I}_z$ ) and denote them by  $|\uparrow\rangle$  and  $|\downarrow\rangle$  with associated energies  $E_\uparrow$  and  $E_\downarrow$  respectively. These states are orthonormal and form a basis for the Hilbert space, such that any initial state can be expressed as

$$\psi(0) = c_\uparrow |\uparrow\rangle + c_\downarrow |\downarrow\rangle. \quad (3.6)$$

When no perturbation is present, this state evolves as

$$\psi(t) = c_\uparrow |\uparrow\rangle e^{-iE_\uparrow t/\hbar} + c_\downarrow |\downarrow\rangle e^{-iE_\downarrow t/\hbar}. \quad (3.7)$$

The idea here is to treat  $c_\uparrow$  and  $c_\downarrow$  as time dependent

$$\psi(t) = c_\uparrow(t) |\uparrow\rangle e^{-iE_\uparrow t/\hbar} + c_\downarrow(t) |\downarrow\rangle e^{-iE_\downarrow t/\hbar}, \quad (3.8)$$

and derive expressions for these under the perturbing Hamiltonian. For the full derivation we refer to Griffiths and Schroeter [11]. The equations for the time-dependent coefficients reduce to

$$c_\uparrow = c_\uparrow(0) - \frac{i}{\hbar} \int_0^t \langle \uparrow | \hat{H}_{rf} | \downarrow \rangle e^{-i(E_\uparrow - E_\downarrow)t'/\hbar} c_\downarrow(t') dt' \quad (3.9)$$

$$c_\downarrow = c_\downarrow(0) - \frac{i}{\hbar} \int_0^t \langle \downarrow | \hat{H}_{rf} | \uparrow \rangle e^{i(E_\uparrow - E_\downarrow)t'/\hbar} c_\uparrow(t') dt'. \quad (3.10)$$

Note the time dependence in the two coefficients  $c_\uparrow(t')$  and  $c_\downarrow(t')$  inside the integral. The idea in time-dependent perturbation theory is to drop this time dependence and iterate, keeping these coefficients constant.

To continue the calculation, we have to specify a control Hamiltonian  $\hat{H}_{rf}$ . The first order approximations for  $c_\uparrow$  and  $c_\downarrow$  are derived using the above expressions and higher order terms are obtained by iteration. Here,

we limit ourselves to the first order. We will choose for  $\mathbf{B}_1(t)$  a circularly polarized field in the x-y-plane such that (analogous to the static field Zeeman Hamiltonian):

$$\hat{H}_{rf} = -\gamma_n \hbar B_1 (\cos(\omega t + \phi) \hat{I}_x - \sin(\omega t + \phi) \hat{I}_y), \quad (3.11)$$

where  $\omega$  and  $B_1$  are the frequency and amplitude of the field, respectively. We also introduced the initial phase  $\phi$  of the magnetic field. Suppose we start out in state  $|\uparrow\rangle$ , so that  $c_\uparrow(0) = 1$  and  $c_\downarrow(0) = 0$ .<sup>1</sup> The upper integral term becomes zero and the lower integral is worked out as follows:

$$c_\downarrow = \frac{i\gamma_n \hbar B_1}{\hbar} \left[ \langle \downarrow | \hat{I}_x | \uparrow \rangle \int_0^t \cos(\omega t' + \phi) e^{i(E_\downarrow - E_\uparrow)t'/\hbar} dt' - \langle \downarrow | \hat{I}_y | \uparrow \rangle \int_0^t \sin(\omega t' + \phi) e^{i(E_\downarrow - E_\uparrow)t'/\hbar} dt' \right]. \quad (3.12)$$

We can simplify the term  $(E_\downarrow - E_\uparrow)/\hbar$ . By inspection of the unperturbed Hamiltonian 3.4 we can see  $E_\downarrow = \frac{1}{2}\gamma_n \hbar B_0$  and  $E_\uparrow = -\frac{1}{2}\gamma_n \hbar B_0$ , keeping in mind that  $I_z$  has eigenvalues  $\pm \frac{1}{2}$ . But then  $(E_\downarrow - E_\uparrow)/\hbar = \gamma_n B_0$  which is the Larmor frequency  $\omega_L$  we defined earlier. Similarly, we set  $\omega_1 = \gamma_n B_1$ . The bra-ket products can also be calculated:

$$c_\downarrow = \frac{i\omega_1}{2} \left[ \int_0^t \cos(\omega t' + \phi) e^{i\omega_L t'} dt' - i \int_0^t \sin(\omega t' + \phi) e^{i\omega_L t'} dt' \right] \quad (3.13)$$

$$c_\downarrow = e^{-i\phi} \frac{i\omega_1}{2} \left[ \int_0^t e^{i(\omega_L - \omega)t'} dt' \right] \quad (3.14)$$

$$c_\downarrow = e^{-i\phi} \frac{\omega_1}{2} \left[ \frac{e^{i(\omega_L - \omega)t} - 1}{\omega_L - \omega} \right]. \quad (3.15)$$

The probability of the system being in state  $|\downarrow\rangle$  at time  $t$  is  $|c_\downarrow|^2$ :<sup>2</sup>

$$|c_\downarrow|^2 = \frac{\omega_1^2}{4} \frac{2 - 2\cos((\omega_L - \omega)t)}{(\omega_L - \omega)^2} \quad (3.16)$$

$$|c_\downarrow|^2 = \frac{\omega_1^2}{4} \frac{\sin^2((\omega_L - \omega)t/2)}{(\omega_L - \omega)^2}. \quad (3.17)$$

Since the state starts out in  $|\uparrow\rangle$ , equation 3.17 describes the probability of transition from  $|\uparrow\rangle$  to  $|\downarrow\rangle$ . This equation tells us a number of things:

1. Transition probability increases as  $|\omega_L - \omega| \rightarrow 0$ . So a field oscillating near the Larmor frequency gives the highest chance of transition. From the formula, the transition probability seems unbounded, but of course this quantity cannot exceed 1. The reason for this is that our assumptions and approximations regarding the perturbation break down: for the circularly polarized magnetic field to count as a perturbation to the Hamiltonian, we need  $B_1 \ll B_0$  and thus  $\omega_1 \ll \omega_L$ .
2. Transition probability increases along with driving field strength (absorbed in  $\omega_1$ ). This is to be expected: a stronger field exerts more torque on the magnetic moment, causing a faster rotation.
3. Transition probability oscillates over time sinusoidally. This means that the highest probability can be attained when  $\sin^2((\omega_L - \omega)t) = 1$ , i.e.  $t = \frac{1}{(\omega_L - \omega)} \left[ \frac{\pi}{2} + n\pi \right]$  with  $n$  integer. But for times  $t = \frac{n\pi}{(\omega_L - \omega)}$ , the system will remain in its original state.
4. Matrix elements of the form  $\langle \psi_i | \hat{H}_{rf} | \psi_j \rangle$  are included in the integral expressions 3.9 and 3.10. Now suppose  $\hat{H}_{rf}$  was a linearly polarized field in the z-direction:

$$\hat{H}_{rf} = -\gamma_n \hbar B_1 \cos(\omega t) \hat{I}_z. \quad (3.18)$$

But since  $\uparrow$  and  $\downarrow$  are eigenstates of  $\hat{I}_z$ , applying this operator to these states would only multiply those states by the corresponding eigenvalue. Since  $\uparrow$  and  $\downarrow$  are also orthogonal, the matrix element is zero. So an oscillating field in the z-direction would not cause a rotation around the z-axis. Another way of viewing this is that if we were to rotate around the z-axis, the states through which we rotate would degenerate. If the states have the same energy, there is no energy difference driving the oscillation.

<sup>1</sup>We could leave  $c_\uparrow$  and  $c_\downarrow$  undefined to derive the formulae for a general state, but for illustration purposes the simpler case of only one nonzero coefficient will suffice.

<sup>2</sup>As calculated earlier, the integral term for  $c_\downarrow$  is equal to zero so  $c_\downarrow$  should remain equal to 1, however  $c_\downarrow$  is not always equal to zero. This violates the normalisation of the state. The inaccuracy stems from the fact that we are using a first order approximation only, whereas higher order terms would give a more accurate value for  $c_\downarrow$ .

Here we derived the effect only for a transition between  $|\uparrow\rangle$  to  $|\downarrow\rangle$  but the derivation is analogous for other states: the difference is in the starting coefficients  $c_{\uparrow}(0)$  and  $c_{\downarrow}(0)$ . The overarching principle is that applying a sinusoidally oscillating field on a certain axis which is orthogonal to the z-axis (together with a static field in the z-direction) causes the (expectation values of the) spin to rotate about that axis. We need the static field because it creates an energy splitting between states, which is necessary to drive an oscillation.

This phenomenon, which is called Rabi oscillation or Rabi flopping is extremely important and lies at the basis of NMR control of nuclear spins. Adjusting pulse length and amplitude carefully allows one to engineer pulse sequences such that a spin can be rotated to any desirable state. It should however be noted that pulses are not perfect and are affected by transient behaviour of the generating apparatus. Such pulse non-idealities will be the subject of discussion in later sections.

We will from now on represent Rabi oscillations only with the corresponding rotation operator, understanding that rotation angles can be translated into pulse times using the Larmor frequency of the system.

### 3.4. The rotating frame

It should be noted that during a Rabi oscillation, the spin is still precessing at the Larmor frequency, which causes the spin to trace out a spiral-shaped path when viewed from the static laboratory frame. This prompts the use of a rotating frame: this frame of reference is rotating at the Larmor frequency when compared to the lab frame, which effectively causes the Larmor precession to disappear in the rotating frame. We will use both frames and we'll try to indicate which frame we are using if this is not clear from context.



# 4

## The nitrogen vacancy center in diamond

In this chapter, we will describe the experimental system which is of interest here, as well as touch on the methods by which this system was simulated as a computer program. Properties of carbon-13 in diamond will be discussed, as well as the nitrogen-vacancy (NV) center point defects which are present alongside carbon. Interactions between carbon-13 nuclei and the NV center and interactions between carbon-13 nuclei (internuclear interactions) are described.

### 4.1. The crystal structure of diamond

Diamond consists of carbon atoms arranged in a face-centered cubic (FCC) lattice which has a two-atom basis. Because of the two-atom basis, the points where carbon atoms (or impurities) are located do not, in the strict mathematical sense, form a lattice themselves. The great majority of the lattice constituents are carbon-12 atoms, which is a spinless isotope of carbon. But approximately 1.1 % of the carbon atoms naturally occur as carbon-13, which does have spin  $\frac{1}{2}$  due to the extra neutron. It turns out that this concentration of nuclei carrying spin in an environment of otherwise spinless nuclei yields a quantum system with very interesting properties for quantum information processing. We can exert control over these nuclei by means of RF-pulses as described in the previous section, as well as use control via point defects in the diamond lattice such as the NV center.

To simulate this in a computer program, the following algorithm was implemented in Python.

1. First, a size for the simulation area is determined. 16 lattice points in all directions defined by the primitive lattice vectors was chosen. Note that the primitive lattice vectors of FCC are not orthogonal so that our simulation area will not be rectangular. This does not matter as we will only be selecting a subset of spins for simulation purposes.
2. The number of carbon-13 nuclei per basis point in the simulation cell was calculated using the number of lattice points and the fixed carbon-13 occurrence proportion of 1.1 %. This number is denoted by  $N$ .
3. The lattice was populated starting from the first basis point at  $(x, y, z) = (0, 0, 0)$ .  $N$  random vectors  $(i, j, k)$  were drawn from a uniform distribution between  $[0, 16)$ . These random vectors were multiplied by the primitive lattice vectors:

$$\mathbf{a}_1 = \frac{a}{2}\hat{x} + \frac{a}{2}\hat{y} \quad (4.1)$$

$$\mathbf{a}_2 = \frac{a}{2}\hat{y} + \frac{a}{2}\hat{z} \quad (4.2)$$

$$\mathbf{a}_3 = \frac{a}{2}\hat{z} + \frac{a}{2}\hat{x}, \quad (4.3)$$

where we introduced the lattice constant of diamond  $a$ , which is equal to 0.3567 nm [12]. The positions resulting from this calculation were stored in an array. The same procedure was repeated for the second basis point at  $(x, y, z) = \frac{1}{4}(a, a, a)$ . Care was taken to ensure carbon-13 atoms do not coincide with the NV center.

A comment on this procedure is that carbon-12 isotopes were ignored and were not placed in the lattice. This is because such nuclei have spin zero and will not have notable interactions with other nuclei.

## 4.2. NV-center

Any physical crystal lattice contains impurities, meaning vacancies in the lattice or atoms which are not isotopes of carbon. An impurity which is of great interest in the scientific community is the Nitrogen-Vacancy (NV) center:

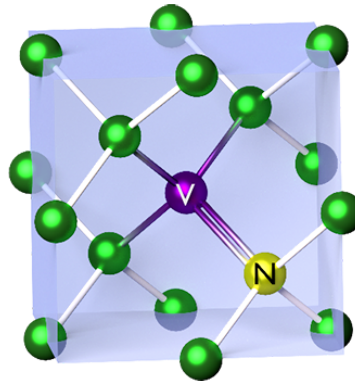


Figure 4.1: A nitrogen-vacancy center in diamond. The configuration pictured above is  $NV^0$ . Sourced from [13].

This point defect, which consists of a nitrogen atom and a neighboring vacancy in the lattice, has a number of interesting properties. NV centers can occur in the  $NV^0$  configuration, where two electrons are provided by the nitrogen atom and three electrons come from the carbon atoms surrounding the vacancy, for a total of five electrons filling the orbitals of the NV center [14]. Such a neutrally charged NV center is pictured in the image above. By capturing another electron, the NV center can become negatively charged. This is known as the  $NV^-$  defect. This thesis will focus on the negatively charged center, which will be referred to as ‘NV center’ from now on.

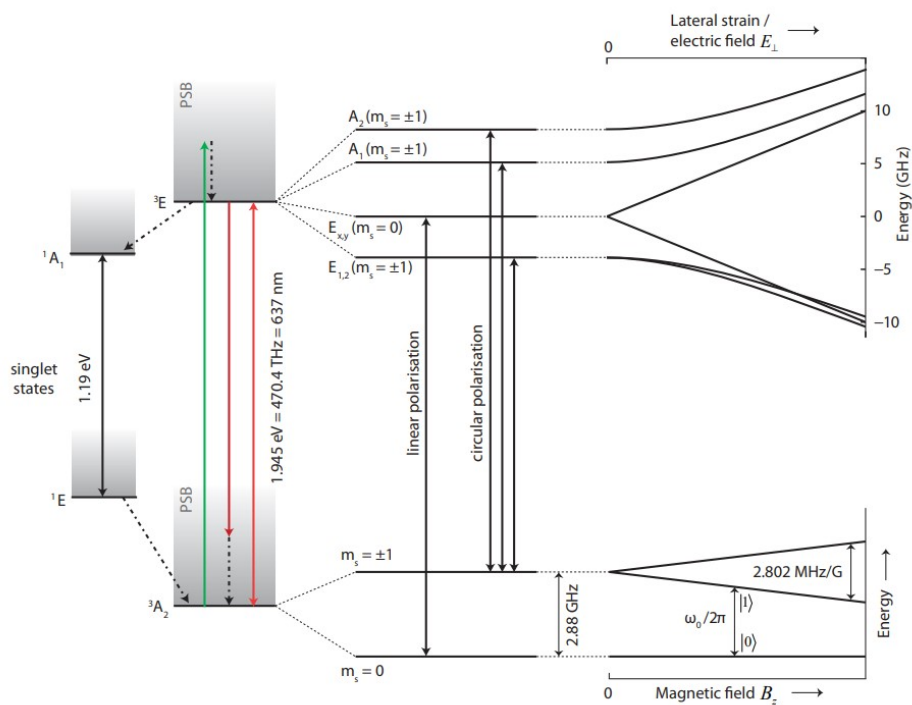


Figure 4.2: The band-structure of the  $NV^-$  center in diamond. Sourced from [15].

The  $^3A_2$  ground state (pictured above on the lower left) is characterized by two orbitals containing two electrons each as well as two degenerate orbitals containing one electron each [16]. The two unpaired electrons form a triplet state ( $S=1$ ) in the ground state due to Coulomb repulsion. Since  $S=1$ , the magnetic spin

number  $m_s$  can take on values  $m_s \in \{-1, 0, 1\}$ . The  $m_s = \pm 1$  levels are separated in energy from  $m_s = 0$  by zero-field splitting, but the two are degenerate unless a static magnetic field is applied. We can define a qubit between the  $m_s = 0$  and  $m_s = -1$  states, where the first state is denoted by  $|0\rangle$  and the second by  $|1\rangle$ . The qubit can be manipulated using microwave spectrum radiation.

In the simulation environment, the nitrogen atom was placed at position:

$$\mathbf{r}_{NV} = 8(\mathbf{a}_1 + \mathbf{a}_2 + \mathbf{a}_3) = 8a(\hat{x} + \hat{y} + \hat{z}). \quad (4.4)$$

The vacancy was placed at position  $8.25a(\hat{x} + \hat{y} + \hat{z})$ . Then, vectors  $\mathbf{r}_{C-NV}$  were calculated which are the distances of the carbon-13 nuclei relative to the NV-center. These are needed for the calculation of interactions.

### 4.3. Dipolar couplings

Dipolar couplings are caused by the magnetic dipole moment of a spin creating a magnetic field, which then has an effect on the magnetic dipole moment of another spin, and vice versa. Define  $\mathbf{r}$  to be the vector between the two dipoles (with the origin on one of these dipoles),  $r$  the magnitude of this vector and  $\mathbf{n}$  the unit vector in the direction of  $\mathbf{r}$ . The magnetic field created by a dipole placed at the origin is [17]:

$$\mathbf{B}_{dip} = \frac{\mu_0}{4\pi} \frac{3(\boldsymbol{\mu} \cdot \mathbf{n})\mathbf{n} - \boldsymbol{\mu}}{r^3}, \quad (4.5)$$

where  $\boldsymbol{\mu}$  is the magnetic moment of the dipole at the origin. Notice that field strength weakens over distance by a factor  $\frac{1}{r^3}$ . Like in the Zeeman Hamiltonian, the Hamiltonian for a dipole  $\boldsymbol{\mu}_1$  in a magnetic field caused by another dipole  $\boldsymbol{\mu}_2$  is then  $-\boldsymbol{\mu}_1 \cdot \mathbf{B}_{dip}^0$ :

$$H_{dip} = -\frac{\mu_0}{4\pi} \frac{\gamma_1 \gamma_2 \hbar^2}{r_{12}^3} [\mathbf{I}_1 \cdot \mathbf{I}_2 - 3(\mathbf{I}_1 \cdot \mathbf{n}_{12})(\mathbf{I}_2 \cdot \mathbf{n}_{12})]. \quad (4.6)$$

When calculating the coupling of a carbon-13 nucleus to the NV-center,  $\gamma_2$  and  $\gamma_1$  denote the gyromagnetic ratios of the electron and of the nucleus, respectively. Simplifying this, we can write the Hamiltonian as

$$H_{e-C} = - \sum_{k \in \{x,y,z\}} \sum_{l \in \{x,y,z\}} A_{kl} S_k I_l, \quad (4.7)$$

where we denoted the spin operator for the electron by  $S_k$  and the  $A_{kl}$  are elements of the following matrix:

$$A = \frac{\mu_0 \gamma_e \gamma_{13C}}{4\pi r^3} \begin{bmatrix} 1 - 3n_x n_x & -3n_x n_y & -3n_x n_z \\ -3n_y n_x & 1 - 3n_y n_y & -3n_y n_z \\ -3n_z n_x & -3n_z n_y & 1 - 3n_z n_z \end{bmatrix}. \quad (4.8)$$

From this matrix, we only take the couplings  $A_{zx}$ ,  $A_{zy}$  and  $A_{zz}$  into account (corresponding to the bottom row of the matrix). The reason for this is that an interaction which changes the expectation value of  $S_z$  for the electron is energetically unfavorable, because the zero-field splitting of the electron (on the order of GHz) is so much greater than the strength of hyperfine interactions in the nuclear spins (on the order of MHz) [18].

Nuclear spins are also coupled to other nuclear spins through the dipolar interaction. In a strong static magnetic field, the Zeeman splitting is typically much larger than internuclear couplings. This prevents internuclear interactions which do not conserve energy from occurring. Interactions which do occur take the form of 'flip-flop' interactions [18]:

$$H_{C-C} = \frac{C_{zz}}{2} [(I_+^1 I_-^2 + I_-^1 I_+^2) - 4I_z^1 I_z^2], \quad (4.9)$$

where we introduced the ladder operators

$$I_{\pm} = I_x \pm iI_y \quad (4.10)$$

and

$$C_{zz} = \frac{\mu_0 \gamma_{13C}^2}{4\pi r_{12}^3} (1 - 3n_z n_z). \quad (4.11)$$

Loosely speaking, the  $I_+$  operator maps  $|\downarrow\rangle$  to  $|\uparrow\rangle$  and  $I_-$  (which is the Hermitian conjugate of  $I_+$ ) does the opposite. The remaining terms in the dipolar coupling Hamiltonian between carbon spins are omitted for

a similar reason as in the case of NV-C interaction. Flip-flop interactions still occur because they preserve energy: both nuclei have (roughly) the same Zeeman splitting between their energy levels so an interaction mediated by  $I_+ I_-$  or  $I_- I_+$  is likely to occur. However, when the NV center is not in the  $|m_s = 0\rangle$  state, these flip-flops do not conserve energy since there is generally a difference in parallel couplings to the NV center between the two spins which is much larger than  $C_{zz}$ . Therefore flip-flop interactions only occur when the NV center is in the  $|m_s = 0\rangle$  state.

The  $I_z I_z$  term commutes with the Zeeman Hamiltonian, so these interactions just raise or lower (depending on the sign of  $C_{zz}$ ) the energy of the Hamiltonian eigenstates.

# 5

## Designing the pulse sequence

This chapter applies the discussed theory to the design of NMR pulse sequences. Such pulse sequences can accomplish a desired effective Hamiltonian to the system, reducing decoherence/and or producing desired simulation conditions. Mathematical techniques such as Average Hamiltonian theory are introduced and motivated. Furthermore, a section on symmetry in pulse design is included.

### 5.1. Average Hamiltonian Theory

An advanced and powerful technique in NMR pulse design is Average Hamiltonian Theory (AHT). The exact mathematical intricacies of this technique are quite involved and out of the scope of this investigation. Therefore we will only touch upon the fundamentals and their implications for pulse design.

The main idea behind AHT is that when looking at a time period  $T$  over which the Hamiltonian of a system is time-dependent, we can instead describe the resulting evolution over that period with a time-independent effective Hamiltonian  $\bar{H}$  [19]. The calculation of this effective Hamiltonian is based on the Magnus expansion [20], which entails a manner of solving differential equations of the form

$$Y'(t) = A(t)Y(t), \quad Y(0) = Y_0 \quad (5.1)$$

by a series of successive approximations. The time-dependent Schrödinger equation (see 2.5) takes on such a form, which is why the Magnus expansion finds great use in quantum mechanics. The effective Hamiltonian  $\bar{H}$  is expanded as follows:

$$\bar{H} = \bar{H}_1 + \bar{H}_2 + \dots, \quad (5.2)$$

where

$$\bar{H}_1 = \frac{1}{T} \int_0^T dt H(t) \quad (5.3)$$

$$\bar{H}_2 = \frac{1}{2iT} \int_0^T dt \int_0^t dt' [H(t), H(t')], \quad (5.4)$$

and so on. When truncating the expression at  $\bar{H}_n$ , a valid Hamiltonian results. Such a Hamiltonian is said to be calculated using  $n$ th order AHT. The goal of this investigation is to design an  $N$ -pulse sequence  $P_m$  [ $0 \leq m \leq N$ ] which is applied to a system, which has time-independent Hamiltonian  $H$ , with free evolution periods  $\tau_m$  in between, such that the effective Hamiltonian over that period is (as close as possible to) a certain desired Hamiltonian. The exact unitary propagator for the system is [5]

$$U(t_b) = e^{-iH\tau_N} P_N \dots e^{-iH\tau_2} P_2 e^{-iH\tau_1} P_1 e^{-iH\tau_0} P_0, \quad (5.5)$$

where the  $P_m$  correspond to tensor products of pulses applied on each individual nuclear spin

$$P_m = P_{m,1} \otimes P_{m,2} \otimes P_{m,3} \otimes \dots, \quad (5.6)$$

where the component pulses  $P_{m,i}$  each take on the form of the rotation operator 2.35. In this thesis, we will consider globally applied pulses (unless indicated otherwise) so that  $P_{m,i} = P_{m,j}$  for all  $i, j$ . Such globally

applied pulses will also be referred to as homogeneous pulse combinations. An extremely important note here is that, in this thesis, the pulses are assumed to be instantaneous and ideal: instantaneous, meaning no actual time is needed to apply the rotation and ideal, signifying a rotation angle and axis which are exactly precise. How realistic these assumptions are will be the subject of later discussion. We can also describe the system in terms of evolution under modified Hamiltonians  $\tilde{H}_k$  [5]:

$$U(t_b) = e^{-i\tilde{H}_N\tau_N} \dots e^{-i\tilde{H}_2\tau_2} e^{-i\tilde{H}_1\tau_1} e^{-i\tilde{H}_0\tau_0}, \quad (5.7)$$

where the  $\tilde{H}_k$  are defined as

$$\tilde{H}_k = U_k^\dagger H U_k, \quad (5.8)$$

with

$$U_k = P_k P_{k-1} \dots P_1 P_0. \quad (5.9)$$

One way of looking at this is that the frame of reference for evolution under the Hamiltonian is effectively rotated by the pulses. Now our first-order term from AHT will look like

$$\tilde{H}_1 = \frac{1}{T} \sum_k \tau_k \tilde{H}_k, \quad (5.10)$$

where the total evolution time is the sum of the intermediate evolution times,  $T = \sum_k \tau_k$ . We will limit ourselves to first-order AHT while mentioning two important properties of the higher-order terms [19]:

1. If  $H(t)$  is symmetric, i.e.  $H(\tau) = H(T - \tau)$  for any  $0 \leq \tau \leq T$ , then all terms in the Magnus expansion which have even order vanish.
2. If  $H(t)$  is antisymmetric, i.e.  $H(\tau) = -H(T - \tau)$  for any  $0 \leq \tau \leq T$ , every term in the Magnus expansion vanishes and the effective Hamiltonian is identically zero.

Due to these properties, it can be said that spatial and temporal symmetry are crucial guiding principles in NMR pulse design.

## 5.2. Rotational symmetries and orientations

The design process of our pulse sequence is based on the 24 rotational symmetries of the cube. The cube can be rotated to any one of 24 positions using only rotations around the x-, y- and z-axes by  $\frac{\pi}{2}$  or multiples thereof. One way of looking at this is that we can rotate any one of the 6 faces of the cube to the top, and then rotate the cube around the z-axis to one of four orientations. Together these actions give us 24 orientations (the identity rotation, i.e. doing nothing, is counted as well). We will denote rotations by the angle with the axis of rotation subscripted:

$$\left[ \frac{\pi}{2} \right]_y. \quad (5.11)$$

In fact, we can use only rotations around the x- and y-axes to accomplish all symmetries: indeed

$$\left[ \frac{-\pi}{2} \right]_x \theta_y \left[ \frac{\pi}{2} \right]_x = \theta_z. \quad (5.12)$$

As was discussed in the section on Rabi oscillations, using pulses we cannot rotate around the z-axis directly due to energy degeneracy. If using only rotations around the x- and y-axes of multiples of  $\frac{\pi}{2}$ , any of these combinations must result in the cube being in one of the 24 orientations.

As one might have guessed, the ‘cube’ which is of interest here is the Hamiltonian of a quantum system. The idea is then to write each of the 24 cube orientations in terms of rotations around x and y, say

$$U_k = \dots P_2 P_1, \quad (5.13)$$

and subsequently represent this as a term

$$\tilde{H}_k = U_k^\dagger H U_k \quad (5.14)$$

in the Magnus expansion and try to optimize for the different times  $\tau_k$ . It should be noted that these  $U_k$  do not directly yield the corresponding pulse sequence. Instead, the  $U_k$  correspond to different orientations and a ‘translation’ step should provide a pulse sequence which rotates through these different orientations. If the goal is complete decoupling,  $\tilde{H} = 0$ , we should aim to incorporate some form of symmetry into the ordering in which the orientations appear such that higher order terms in the Magnus expansion will tend to cancel out. A similar way of thinking was formalized by Choi et al. [21].

### 5.3. Linear Programming in NMR pulse design

Approaching NMR pulse design from a Linear Programming (LP) perspective was pioneered by O’Keeffe et al. [5] in 2019. The method described below is heavily inspired upon the work of these authors.

The first step is to compute the Pauli projection as described in equation 2.29 for each of our AHT terms  $\tilde{H}_k$ :

$$\mathcal{P}(\tilde{H}_k) = \begin{bmatrix} c_1 \\ c_2 \\ \vdots \\ c_{4^n} \end{bmatrix}, \quad (5.15)$$

where  $n$  denotes the number of qubits in the system, corresponding to a  $2^n \times 2^n$  Hamiltonian. Which coefficient corresponds to which tensor product of Pauli matrices does not actually matter, as long as we use the same mapping for all the projections. We insert the projections of our  $\tilde{H}_k$  as column vectors into a matrix  $A$ :

$$A = [\mathcal{P}(\tilde{H}_1) \quad \mathcal{P}(\tilde{H}_2) \quad \cdots \quad \mathcal{P}(\tilde{H}_{23}) \quad \mathcal{P}(\tilde{H}_{24})]. \quad (5.16)$$

The result is a  $4^n \times 24$  matrix. Remember that the Pauli projection is linear, so the Pauli projection of  $\tilde{H}_1$  will be the weighted sum of the Pauli projections of the  $\tilde{H}_k$  respectively:

$$\mathcal{P}(\tilde{H}_1) = \mathcal{P}\left(\frac{1}{T} \sum_k \tau_k \tilde{H}_k\right) = \frac{1}{T} \sum_k \tau_k \mathcal{P}(\tilde{H}_k). \quad (5.17)$$

In first order AHT, only the relative lengths of the evolution periods are of importance and not necessarily the actual times themselves. Therefore the total evolution time  $T$  can be scaled arbitrarily and we set it to 1 for convenience:

$$\mathcal{P}(\tilde{H}_1) = \sum_k \tau_k \mathcal{P}(\tilde{H}_k), \quad (5.18)$$

where we enforce the constraint

$$\sum_k \tau_k = 1. \quad (5.19)$$

Note however that this indifference to time scale does not hold up in higher order AHT and indeed in real-life systems. Such non-idealities determine the actual performance of the decoupling method and will be the subject of discussion of the following sections in this thesis.

If we now store the  $\tau_k$  in a column vector we can elegantly express the resulting Hamiltonian from first-order AHT:

$$\mathcal{P}(\tilde{H}_1) = [\mathcal{P}(\tilde{H}_1) \quad \mathcal{P}(\tilde{H}_2) \quad \cdots \quad \mathcal{P}(\tilde{H}_{23}) \quad \mathcal{P}(\tilde{H}_{24})] \begin{bmatrix} \tau_1 \\ \tau_2 \\ \vdots \\ \tau_{23} \\ \tau_{24} \end{bmatrix} \equiv A\boldsymbol{\tau}. \quad (5.20)$$

Now we have to define our target Hamiltonian. We can split the original Hamiltonian into a non-desirable and a desirable part:

$$H = H_0 + H_1, \quad (5.21)$$

where we want to keep  $H_1$  and discard  $H_0$ :

$$A\boldsymbol{\tau} = 0 \cdot \mathcal{P}(H_0) + \beta \mathcal{P}(H_1), \quad (5.22)$$

where  $\beta$  is a coefficient between 0 and 1 which signifies the ‘weakening’ of system dynamics under application of pulses [5]. The goal is then to bring  $\beta$  as close as possible to 1 as possible. The power behind the LP-approach lies in the fact that these two component Hamiltonians can be tuned to include or exclude any combination of system dynamics. It should be noted however, that the resulting system is not always feasible. For this thesis the main goal is decoupling so that  $H_0 = H$ ,  $H_1 = 0$ :

$$A\boldsymbol{\tau} = 0 \cdot \mathcal{P}(H_0) + \beta \mathcal{P}(H_1) = \mathbf{0}. \quad (5.23)$$

We append the constraint on the sum over  $\tau_k$  to this matrix equation:

$$\begin{bmatrix} \mathcal{P}(\tilde{H}_1) & \mathcal{P}(\tilde{H}_2) & \cdots & \mathcal{P}(\tilde{H}_{23}) & \mathcal{P}(\tilde{H}_{24}) \\ 1 & 1 & \cdots & 1 & 1 \end{bmatrix} \boldsymbol{\tau} = \begin{bmatrix} 0 \\ 0 \\ \vdots \\ 0 \\ 1 \end{bmatrix}. \quad (5.24)$$

However, finding a strict solution to this system might be infeasible: it could be the case that the Pauli coefficients do not sum exactly to zero for any  $\boldsymbol{\tau}$ . Therefore we want to define some measure of ‘closeness’ to the target Hamiltonian and optimize for this accordingly. A straightforward way of doing this is to add slack variables. To each row corresponding to the Pauli coefficients, two slack variables are added. We will call these slack variables  $\epsilon_1$  and  $\epsilon_2$ . One of these is added to the sum of Pauli coefficients and one is subtracted: this way we can optimize using only positive variables, while still adapting for both positive and negative deviations. The resulting ensemble takes on the following form:

$$\begin{bmatrix} \mathcal{P}(\tilde{H}_1) & \mathcal{P}(\tilde{H}_2) & \cdots & \mathcal{P}(\tilde{H}_{23}) & \mathcal{P}(\tilde{H}_{24}) & I & -I \\ 1 & 1 & \cdots & 1 & 1 & \mathbf{0}^T & \mathbf{0}^T \end{bmatrix} \begin{bmatrix} \boldsymbol{\tau} \\ \boldsymbol{\epsilon}_1 \\ \boldsymbol{\epsilon}_2 \end{bmatrix} = \begin{bmatrix} 0 \\ 0 \\ \vdots \\ 0 \\ 1 \end{bmatrix}. \quad (5.25)$$

We would like to minimize the sum of the slack variables, penalizing positive and negative deviations equally:

$$\min [0 \quad \cdots \quad 0 \quad 1 \quad 1 \quad \cdots \quad 1 \quad 1] \begin{bmatrix} \boldsymbol{\tau} \\ \boldsymbol{\epsilon}_1 \\ \boldsymbol{\epsilon}_2 \end{bmatrix}, \quad (5.26)$$

where the min stands for minimization. Linear programming libraries are widely available and well-implemented in many programming languages. The above LP-formulation was implemented in Python.

## 5.4. Symmetry considerations

Symmetry is an integral part of quantum mechanics and invites elegant but elusive mathematics into the field. A discussion of symmetry in NMR pulse design would indeed be extensive enough for a paper on its own [22]. Since it is so important to NMR pulse design, we will explain the thought process behind the symmetry considerations for the pulse sequence using a toy example of a 1-qubit system. The calculation is somewhat tedious but the end result is quite enlightening.

Suppose we have a 1-qubit system. The Hamiltonian  $H$  can then be decomposed into the four Pauli matrices:<sup>1</sup>

$$H = a\sigma_0 + b\sigma_x + c\sigma_y + d\sigma_z. \quad (5.27)$$

Compare to equation 2.29 where we put a factor  $\frac{1}{2}$  in front of the representation. This choice is arbitrary: including or excluding the prefactor facilitates easier handling in the first and second case respectively. The unitaries  $U_k$  which are applied to the Hamiltonian are (products of) rotation operators. Let’s limit ourselves to one rotation operation around the x-axis for illustration purposes. The AHT term  $\tilde{H}_k$  is defined as

$$\tilde{H}_k = U_k^\dagger H U_k. \quad (5.28)$$

We substitute the x-axis rotation operator for  $U_k$ , using the form derived in 2.37:

$$\tilde{H}_k = \left[ \cos \frac{\theta}{2} I + i \sin \frac{\theta}{2} \sigma_x \right] H \left[ \cos \frac{\theta}{2} I - i \sin \frac{\theta}{2} \sigma_x \right]. \quad (5.29)$$

Let’s set  $\cos \frac{\theta}{2} = \alpha$ ,  $\sin \frac{\theta}{2} = \beta$ :

$$\tilde{H}_k = (\alpha\sigma_0 + i\beta\sigma_x)H(\alpha\sigma_0 - i\beta\sigma_x) \quad (5.30)$$

<sup>1</sup>That is, including the identity matrix  $\sigma_0$

and fill in the Pauli decomposition of  $H$

$$\tilde{H}_k = (\alpha\sigma_0 + i\beta\sigma_x)(a\sigma_0 + b\sigma_x + c\sigma_y + d\sigma_z)(\alpha\sigma_0 - i\beta\sigma_x), \quad (5.31)$$

which we can work out using the properties of Pauli matrices stated in section 2.4:

$$\tilde{H}_k = (\alpha\sigma_0 + i\beta\sigma_x)(\alpha(a\sigma_0 + b\sigma_x + c\sigma_y + d\sigma_z) - i\beta(b\sigma_0 + a\sigma_x + id\sigma_y - ic\sigma_z)) \quad (5.32)$$

$$\begin{aligned} \tilde{H}_k &= \alpha^2(a\sigma_0 + b\sigma_x + c\sigma_y + d\sigma_z) - i\alpha\beta(b\sigma_0 + a\sigma_x + id\sigma_y - ic\sigma_z) \\ &\quad + i\alpha\beta(b\sigma_0 + a\sigma_x - id\sigma_y + ic\sigma_z) + \beta^2(a\sigma_0 + b\sigma_x - c\sigma_y - d\sigma_z). \end{aligned} \quad (5.33)$$

A lot of the terms drop out, keeping in mind that  $\alpha^2 + \beta^2 = 1$ :

$$\tilde{H}_k = a\sigma_0 + b\sigma_x + (\alpha^2 - \beta^2)(c\sigma_y + d\sigma_z) + 2\alpha\beta(d\sigma_y - c\sigma_z). \quad (5.34)$$

The calculation is completely analogous for the other rotation axes. The end result is the same, with x, y and z cyclically permuted. A couple of observations:

1. The Pauli coefficients of  $\sigma_0$  and  $\sigma_x$  remain unchanged.
2.  $\alpha = 0$  corresponds to a rotation by  $\pi$ , which causes the coefficients in front of  $\sigma_y$  and  $\sigma_z$  to become negative.  $\beta = 0$  is the trivial identity rotation.
3. A  $\pm\frac{\pi}{2}$  rotation corresponds to the flipping of the coefficients in front of  $\sigma_y$  and  $\sigma_z$  with one of these becoming negative, depending on the sign of the rotation.

Remember that in AHT, all terms completely vanish if the Hamiltonian  $H(t)$  is antisymmetric in time. Putting this all together, this means:

**By rotating over a certain axis, we can switch around and/or change the signs of the Hamiltonian components along the other two axes.**

This principle lies at the heart of this pulse sequence design. We cannot, however, cancel the identity part of the Hamiltonian. But the interactions we are interested in cancelling are mediated by the spin matrices, and not by the identity matrix.

Let's translate these findings to a set of rules for the application of pulses. Suppose we start with x- y- and z-Pauli coefficients b, c, d. They are transformed by the different pulses in the following manner:

1.  $[\frac{\pi}{2}]_x : (b, c, d) \rightarrow (b, d, -c)$ .
2.  $[\frac{\pi}{2}]_y : (b, c, d) \rightarrow (-d, c, b)$ .
3.  $[\frac{\pi}{2}]_z : (b, c, d) \rightarrow (c, -b, d)$ .
4.  $[\pi]_x : (b, c, d) \rightarrow (b, -c, -d)$ .
5.  $[\pi]_y : (b, c, d) \rightarrow (-b, c, -d)$ .
6.  $[\pi]_z : (b, c, d) \rightarrow (-b, -c, d)$ .

Keep in mind that the z-pulse is actually accomplished by combining x- and y-pulses: we cannot actually rotate around the z-axis since the static field is applied in that direction, causing energy degeneration in the x-y plane. However, z-pulses are much more convenient in notation. This 'library' of pulses is completed by noting that a  $[-\frac{\pi}{2}]_i$  rotation is equal to a  $[\frac{\pi}{2}]_i$  and a  $[\pi]_i$  rotation applied consecutively.<sup>2</sup> Using these rules we can construct a table to represent all 24 rotational symmetries of the cube in this way:

	id	$[\frac{\pi}{2}]_x$	$[\frac{\pi}{2}]_y$	$[-\frac{\pi}{2}]_y$	$[-\frac{\pi}{2}]_x$	$[\pi]_x$
id	(b, c, d)	(b, d, -c)	(-d, c, b)	(d, c, -b)	(b, -d, c)	(b, -c, -d)
$[\frac{\pi}{2}]_z$	(c, -b, d)	(d, -b, -c)	(c, d, b)	(c, -d, -b)	(-d, -b, c)	(-c, -b, -d)
$[-\frac{\pi}{2}]_z$	(-c, b, d)	(-d, b, -c)	(-c, -d, b)	(-c, d, -b)	(d, b, c)	(c, b, -d)
$[\pi]_z$	(-b, -c, d)	(-b, -d, -c)	(d, -c, b)	(-d, -c, -b)	(-b, d, c)	(-b, c, -d)

Table 5.1: Rotations of the cube represented in terms of permutations of coefficients. The rotation corresponding to the column of the entry is applied first.

<sup>2</sup>This holds only when pulses are ideal and instantaneous.

which is somewhat overwhelming. If we colour the entries which have the same permutation of letters, but with different signs, a pattern is shown:

	id	$[\frac{\pi}{2}]_x$	$[\frac{\pi}{2}]_y$	$[-\frac{\pi}{2}]_y$	$[-\frac{\pi}{2}]_x$	$[\pi]_x$
id	(b, c, d)	(b, d, -c)	(-d, c, b)	(d, c, -b)	(b, -d, c)	(b, -c, -d)
$[\frac{\pi}{2}]_z$	(c, -b, d)	(d, -b, -c)	(c, d, b)	(c, -d, -b)	(-d, -b, c)	(-c, -b, -d)
$[-\frac{\pi}{2}]_z$	(-c, b, d)	(-d, b, -c)	(-c, -d, b)	(-c, d, -b)	(d, b, c)	(c, b, -d)
$[\pi]_z$	(-b, -c, d)	(-b, -d, -c)	(d, -c, b)	(-d, -c, -b)	(-b, d, c)	(-b, c, -d)

Table 5.2: Rotations of the cube represented in terms of permutations of coefficients. The rotation corresponding to the column of the entry is applied first. Entries are coloured according to permutation of letters.

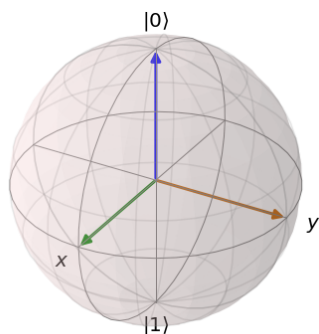


Figure 5.1: Normal right-handed coordinate system.

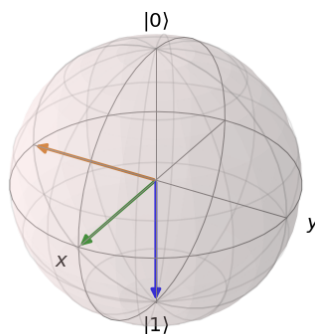


Figure 5.2: Right-handed coordinate system flipped by  $\pi$  over the x-axis.

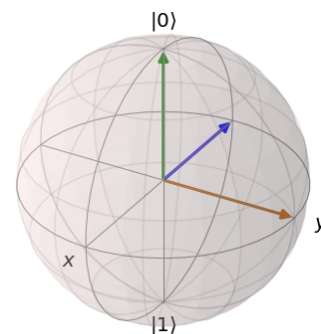


Figure 5.3: Right-handed coordinate system flipped by  $\frac{\pi}{2}$  over the y-axis.

Evidently, some sort of symmetry appears. Notice that any entry of a colour is equal to any other entry of that same colour, but with exactly two of the signs flipped. A natural question which arises is why none of the entries are exactly equal to another entry multiplied by -1. If this were the case, we would be able to pair up orientations in such a way that our Hamiltonian is completely antisymmetric in time, guaranteeing that all AHT terms are identically zero. Such entries do not appear because such an orientation is actually prohibited: a coordinate system cannot be rotated in such a way that all its axes are flipped: compare figure 5.1 to figure 5.2. Doing so would require a mirroring operation. If we were to include mirroring symmetries of the cube, these would add another 24 elements to the group described in table 5.2 above. These mirrorings and rotations together form the octahedral group of 48 elements, describing all symmetries of the cube. However, mirroring operations cannot be accomplished by (combinations of) rotations. That's why we can only hope for some sort of symmetry, and not a perfect (i.e. antisymmetric) one.

Another way of looking at the previous statement is by looking at the number of operations. If we consider one operation to be either changing the sign of one component or switching two components around, the allowed pulses each consist of 2 operations. So each pulse sequence must consist of an even number of operations. But flipping the sign of all three entries constitutes an odd number of operations, which can then never be accomplished by multiples of an even number of operations.

If we 'read' the table in the order in which the orientations are applied, we see that the resulting Hamiltonians (that is, the  $\tilde{H}_k$ ) are partly symmetric and partly antisymmetric. Therefore we can expect a great deal of the higher-order AHT terms to vanish. This will result in an effective Hamiltonian which is close to zero.

However, in NMR it is generally wise to keep the pulse sequence as short as possible. Therefore we can select only certain entries from the table such that the sequence is symmetric. This gives rise to a whole family of pulse sequences. We can now also intuitively guess which combinations of orientations give rise to a useful pulse sequence by combining similar entries.

## 5.5. Internuclear interactions

One thing to keep in mind is that all of the above was derived for a 1-qubit system, which is hardly representative for real-life situations. The Hamiltonian of an  $n$ -qubit system with  $n > 1$  will not be merely a tensor product of the individual qubit Hamiltonians, but will include cross-terms as well because of internuclear

interactions. We will look at look at the interactions between two qubits as defined in chapter 4 and how one could go about cancelling these.

Referring to equation 4.9, we have

$$H_{C-C} = \frac{C_{zz}}{2} [(I_+^1 I_-^2 + I_-^1 I_+^2) - 4I_z^1 I_z^2]. \quad (5.35)$$

Expanding the equation using the definition of the ladder operators:

$$H_{C-C} = \frac{C_{zz}}{2} [(I_x^1 + iI_y^1)(I_x^2 - iI_y^2) + (I_x^1 - iI_y^1)(I_x^2 + iI_y^2) - 4I_z^1 I_z^2], \quad (5.36)$$

which is rewritten as

$$H_{C-C} = C_{zz}(I_x^1 I_x^2 + I_y^1 I_y^2 - 2I_z^1 I_z^2). \quad (5.37)$$

Suppose we apply a homogeneous pulse combination (i.e. the same pulse for all qubits) on the system. For example, we can apply a  $[\pi]_x$  pulse on every nuclear spin. According to the symmetry rules, the result will be the following:

$$H'_{C-C} = C_{zz}(I_x^1 I_x^2 + (-I_y^1)(-I_y^2) - 2(-I_z^1)(-I_z^2)), \quad (5.38)$$

which is equal to the expression we had before. If, however, we were to apply the  $[\pi]_x$  pulse only on the first spin we would have a useful result:

$$H''_{C-C} = C_{zz}(I_x^1 I_x^2 - I_y^1 I_y^2 + 2I_z^1 I_z^2). \quad (5.39)$$

Now, compared to the original Hamiltonian  $H_{C-C}$ , the signs of the y- and z- spin operators have been flipped. This provides (at least some) cancellation of internuclear interactions.

The problem however with applying such heterogeneous pulse combinations in practice is that every nuclear spin is coupled to every nuclear spin which is different from itself. Indeed, if the system at hand were a 'spin chain', where every spin only has internuclear interactions with its (two or one) nearest neighbors, we could apply  $\pi$ -pulses to every other spin to achieve decoupling. But a system with more complex couplings requires accordingly complex pulse schemes. For simplicity, we would prefer to decouple the system using globally applied pulses. These homogeneous pulse combinations will be the focus on the rest of this thesis. Heterogeneous pulse combinations are treated in the discussion section.

Let's see what happens if we apply a  $[\frac{\pi}{2}]_x$  pulse instead on Hamiltonian 5.37:

$$H'''_{C-C} = C_{zz}(I_x^1 I_x^2 - 2I_y^1 I_y^2 + I_z^1 I_z^2). \quad (5.40)$$

The  $\frac{\pi}{2}$ -pulse flipped the coefficients corresponding to the z- and y- spin operators (the sign changes cancel each other out). Similar effects will occur when applying  $\frac{\pi}{2}$ -pulses around the other y-axis. A  $\frac{\pi}{2}$ -pulse around the z-axis would not change the effective Hamiltonian, but such rotations cannot be implemented directly anyway. For this reason,  $\frac{\pi}{2}$ -pulses around the x- and y-axes are particularly useful for cancelling internuclear interactions when applied globally. The requirement for pulses around these angles for carbon-carbon decoupling indeed corresponds to existing research [21].



# 6

## Results

We will now optimize the evolution times for each of the orientations described in table 5.2. We can restrict the search space to define different maximal sequence lengths. The corresponding evolution times are calculated by solving the LP-formulation. Then we will compute the performance of the obtained pulse sequences by propagating the system over the evolution period. This is done by means of applying unitaries corresponding to the calculated evolution times followed by unitaries corresponding to the prescribed pulse rotations. We choose the 5 qubits with the largest parallel coupling to the NV center since these will be the most interesting for control and readout. All qubits will start out in the  $|+x\rangle$  state:

$$\rho(t=0) = \bigotimes_{1 \leq i \leq n} |+x\rangle \langle +x| = \frac{1}{2^n} \begin{pmatrix} 1 & \cdots & 1 \\ \vdots & \ddots & \vdots \\ 1 & \cdots & 1 \end{pmatrix}. \quad (6.1)$$

Moreover, a static magnetic field of 403.553 Gauss will be applied. We will study evolution both with the NV center fixed in the  $|m_s = -1\rangle$  state and in the  $|m_s = 0\rangle$  state. Of these two, the performance under the  $|m_s = -1\rangle$  state is perhaps the most interesting because the parallel and perpendicular couplings to the NV center need to be cancelled out as well.

Furthermore we will look at the  $n$  qubits which have the strongest parallel interaction with the NV center because these provide the most interesting targets for readout and control.

To determine the performance of the pulse sequence, we have to define some metric. We are interested in complete decoupling such that the effective Hamiltonian over the whole evolution period is zero. A zero Hamiltonian corresponds to a unitary propagator which is identity, therefore we should expect the system to be in the  $\rho(t=0)$  state at the end of the pulse sequence. The goal is then to scale the evolution period to as large as possible without deviating significantly from the starting state. To quantify this, we will compute the matrix fidelity as described in the first chapter, with regard to the density matrix  $\rho(t=0)$  as given in equation 6.1. The matrix fidelity will be the leading performance metric here, as this statistic is calculated using the entire density matrix, whereas expectation values are only calculated by tracing over a single qubit. The obtained sequences will be compared to the ‘WAHUHA+echo’ sequence [21], which is a six-pulse sequence commonly used in NMR for decoupling. Both sequences will also be compared to the baseline, i.e. free evolution without applying any pulses.

### 6.1. Pulse sequence 1: 24 orientations

Using the approach described above, the linear program yielded the following optimal values for  $\tau$ :

$$\tau = \frac{1}{24} \begin{bmatrix} 1 \\ 1 \\ \vdots \\ 1 \\ 1 \end{bmatrix}. \quad (6.2)$$

This result is in accordance with the theory we developed in the previous chapter. We should expect some sort of symmetry in the derived evolution times. Since the 24 orientations can be split up into six different ‘groups’<sup>1</sup> containing four orientations each, we would expect to spend equal time in each of these orientations, at least within such a symmetric group. Remember that  $\tau$  is normalized and we can adapt the relative times to the desired timescale.

The pulse sequence which actually produces this succession of orientations was determined by a brute-force program<sup>2</sup>. This yields the following pulse sequence:

$$\begin{aligned} &-\tau - \left[\frac{\pi}{2}\right]_x - \tau - \left[-\frac{\pi}{2}\right]_x \left[\frac{\pi}{2}\right]_y - \tau - [\pi]_y - \tau - \left[\frac{\pi}{2}\right]_y \left[-\frac{\pi}{2}\right]_x - \tau - \left[-\frac{\pi}{2}\right]_x - \tau - \left[\frac{\pi}{2}\right]_x \left[-\frac{\pi}{2}\right]_y \left[\frac{\pi}{2}\right]_x - \tau - \left[-\frac{\pi}{2}\right]_y - \tau - \left[\frac{\pi}{2}\right]_y \left[\frac{\pi}{2}\right]_x \\ &-\tau - [\pi]_x - \tau - \left[\frac{\pi}{2}\right]_x \left[\frac{\pi}{2}\right]_y - \tau - \left[\frac{\pi}{2}\right]_y - \tau - [\pi]_x - \tau - \left[\frac{\pi}{2}\right]_y - \tau - \left[-\frac{\pi}{2}\right]_y \left[-\frac{\pi}{2}\right]_x - \tau - [\pi]_x - \tau - \left[-\frac{\pi}{2}\right]_x \left[-\frac{\pi}{2}\right]_y - \tau - \left[-\frac{\pi}{2}\right]_y \\ &-\tau - \left[\frac{\pi}{2}\right]_x \left[-\frac{\pi}{2}\right]_y \left[\frac{\pi}{2}\right]_x - \tau - \left[-\frac{\pi}{2}\right]_x - \tau - \left[\frac{\pi}{2}\right]_x \left[-\frac{\pi}{2}\right]_y - \tau - [\pi]_y - \tau - \left[-\frac{\pi}{2}\right]_y \left[\frac{\pi}{2}\right]_x - \tau - \left[\frac{\pi}{2}\right]_x - \tau - [\pi]_y \end{aligned}$$

Here  $\tau$  signifies a free evolution period with length equal to 1/24 of total evolution time. We will refer to this sequence as A-24.

Matrix fidelity for evolution times between 0-1 ms showed the following patterns:

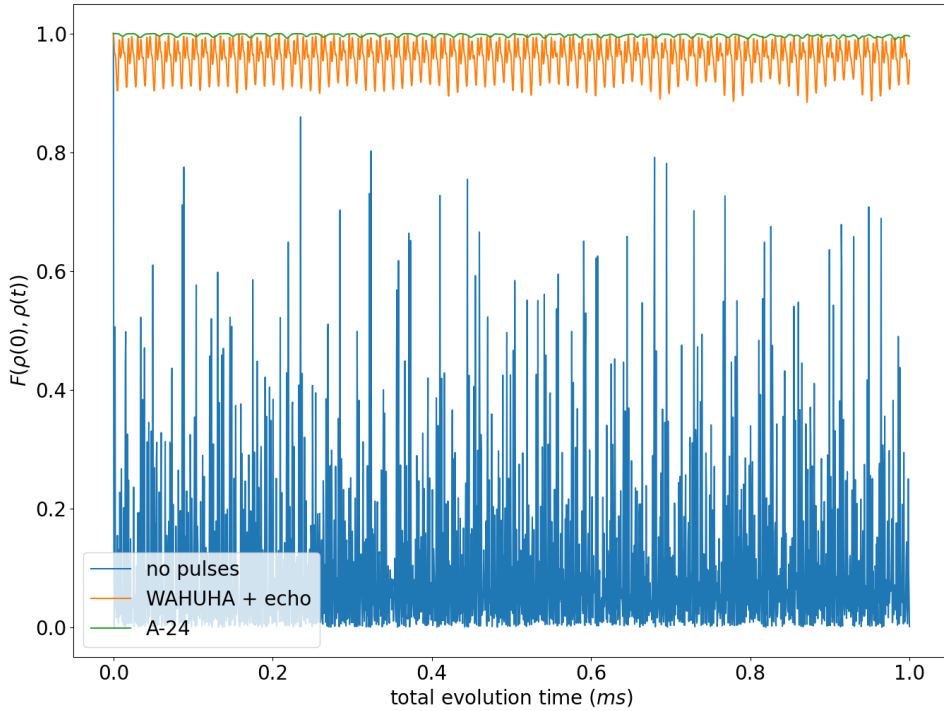


Figure 6.1: Fidelity for evolution without pulses, C-24 and WAHUHA + echo pulse sequences for total evolution time 1 ms. NV center was fixed in  $|m_s = -1\rangle$  state.

Clearly, both the WAHUHA + echo and A-24 sequence are an improvement over free evolution. For the baseline case where no pulses are applied, the matrix fidelity drops almost instantly, corrupting the quantum state beyond usability. The reason for this is the large difference in NV couplings among the qubits. These differences in couplings are roughly on the order of  $10^5$  Hz, corresponding to a characteristic interaction timescale of  $10 \mu\text{s}$  which causes a rapid decrease in fidelity. From now on we will omit the plot for fidelity when no pulses are applied. This way we can view the behavior of fidelity under pulse sequences more clearly and scale the y-axis more appropriately:

<sup>1</sup>Group is not used in the strictly mathematical sense here.

<sup>2</sup>In principle, we could determine the shortest pulse sequences to transfer between orientations from table 5.2. However, a brute-force method, i.e. trying out all combinations of up to 3 rotations, carries the advantage of not having to convert between the permutation representation and the actual rotation matrices. Furthermore, the speed gain from an algebraic approach over the brute-force method is negligible.

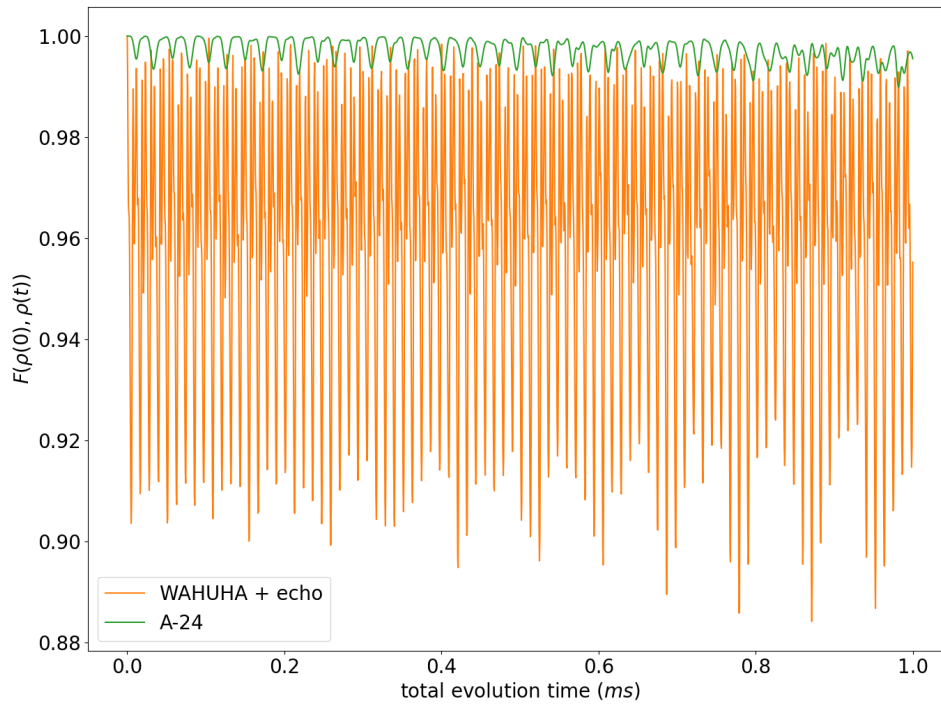


Figure 6.2: Fidelity for A-24 and WAHUHA + echo pulse sequences for total evolution time 1 ms. NV center was fixed in  $|m_s = -1\rangle$  state.

On the timescale which is plotted above, A-24 seems to be more effective than WAHUHA + echo at retaining fidelity for longer timescales. The oscillation in fidelity for both sequences signifies that some (parts of) interactions are not cancelled out and disturb the quantum state. Comparing A-24 and WAHUHA + echo, A-24 cancels out high-frequency oscillations to a greater degree.

We can look at a larger timescale to see how the two sequences perform:

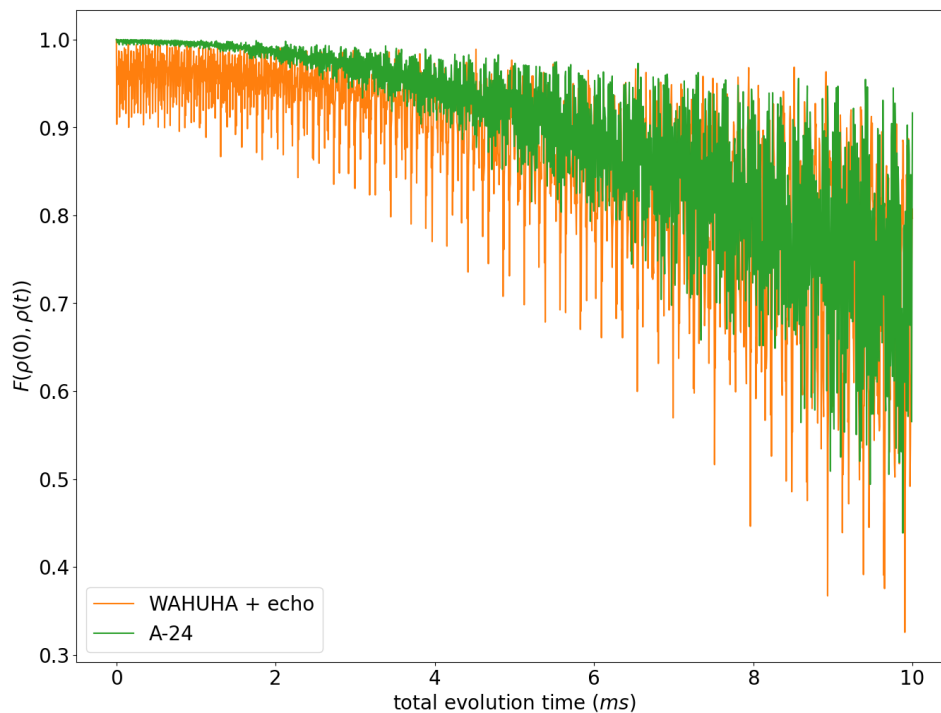


Figure 6.3: Fidelity for A-24 and WAHUHA + echo pulse sequences for total evolution time 10 ms. NV center was fixed in  $|m_s = -1\rangle$  state.

Again, A-24 outperforms WAHUHA + echo for timescales up to 5 ms. After this time, the difference is not so clear and both sequences begin to devolve into chaos.

The deterioration in fidelity was verified using Mathematica to rule out numerical errors. This was done for WAHUHA + echo since this sequence has been proven to cancel out internuclear and carbon-NV interactions to at least some degree. Therefore it serves as a baseline for verification of the validity of the experimental results. The pattern which was obtained indeed matched the rate of deterioration in fidelity which was demonstrated above. The obtained analytical expression for fidelity can be found in the appendix.

With the NV center in the  $|m_s = 0\rangle$  state, only internuclear interactions and Larmor precession are present. Over a timescale of 1 ms, the following pattern showed:

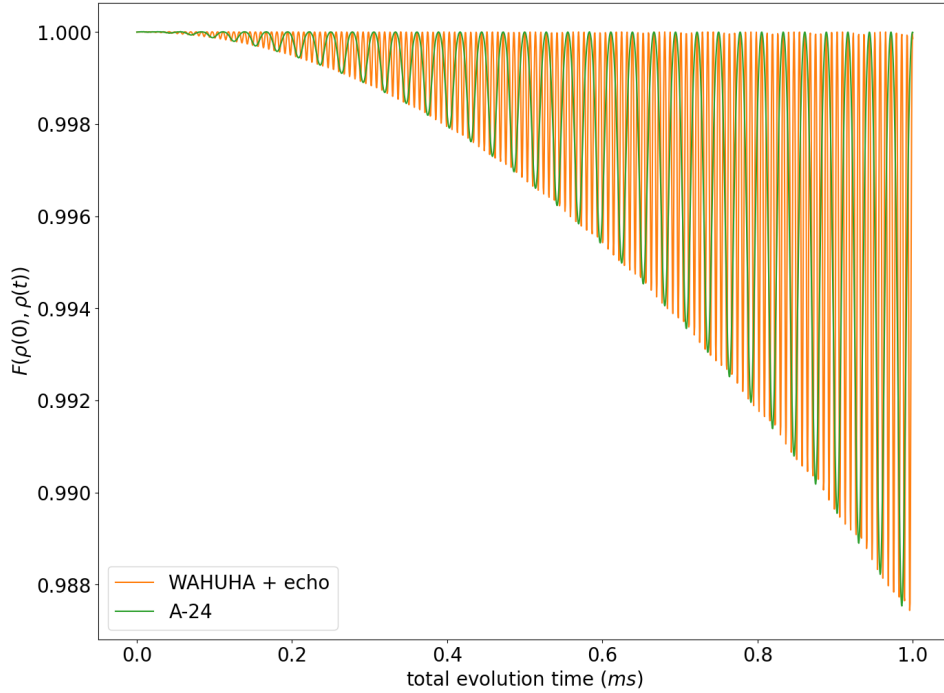


Figure 6.4: Fidelity for A-24 and WAHUHA + echo pulse sequences for total evolution time 1 ms. NV center was fixed in  $|m_s = 0\rangle$  state.

The resulting fidelity is a slow oscillation modulated by a fast oscillation. The fast oscillation turns out to be 1/12 the Larmor frequency for A-24, and 1/3 the Larmor frequency for WAHUHA + echo. The difference between these harmonics is proportional to the number of evolution periods: WAHUHA + echo has 6 whereas A-24 has 24. The slow oscillation is a remaining component of the internuclear interaction, clearly showing non-ideal cancellation of this effect for both sequences.

Notably, deterioration of fidelity is roughly equal for both sequences, with the difference being that the WAHUHA + echo sequence contains a higher frequency oscillation in fidelity because of its relatively longer evolution periods. Thus, A-24 will not outperform the existing sequence regarding cancellation of Larmor frequency and internuclear interactions, but does provide a more effective approach to cancellation of NV center interactions. Since the latter interactions usually manifest on a shorter timescale than internuclear interactions, A-24 might have an advantage over WAHUHA + echo in protecting quantum states from decoherence on a millisecond timescale. Ineffective cancellation of Larmor precession can be mitigated (for both sequences) by selecting evolution times according to the periodicity of fidelity as shown above.

Because fidelity is deteriorating visibly at roughly the timescale of internuclear couplings (1-10 ms timescale), one might wonder if internuclear interactions are being cancelled at all. We can evolve the qubits only according to the Hamiltonian resulting from these interactions (i.e. no couplings to NV center and no Larmor precession) to see the effect:

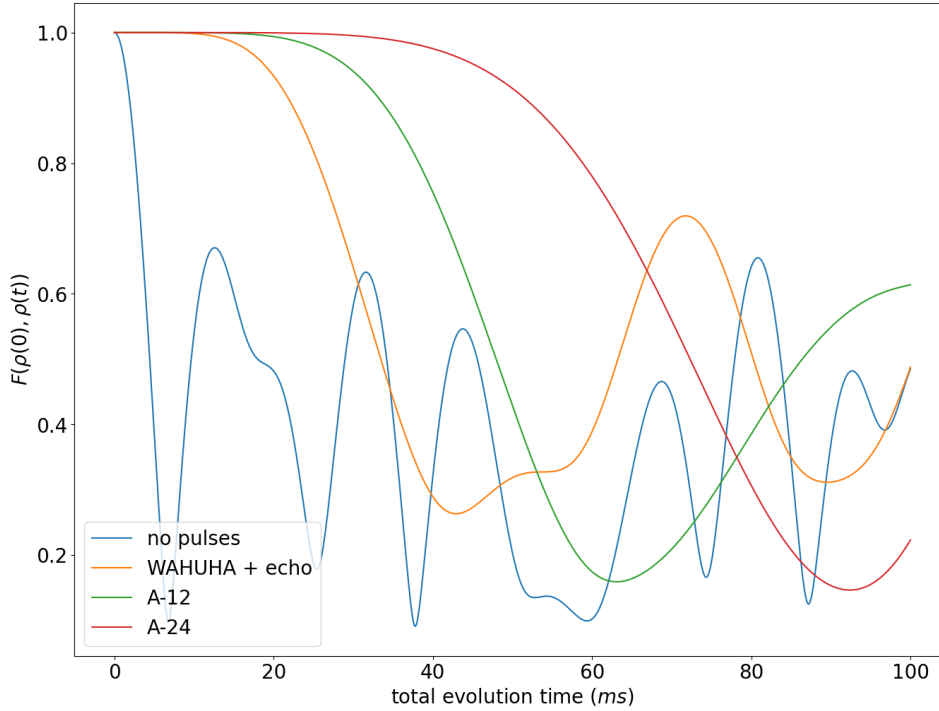


Figure 6.5: Fidelity for no pulses, A-24, A-12 and WAHUHA + echo pulse sequences for total evolution time 100 ms. Evolution according to only internuclear interactions.

We see that the pulse sequences did indeed have an effect on the stability under internuclear interactions. Note the lengthened timescale here to accommodate the slower interactions. Of the three pulse sequences, A-24 seems to be the most effective, followed by A-12 and then WAHUHA + echo. On the timescales studied in the previous sections, internuclear interactions seem to be cancelled out quite effectively by the designed pulse sequences. The drop in fidelity can therefore be attributed to a chaotic effect caused by the presence of a large plurality of couplings, which differ for every qubit. The combination of all these different couplings then causes the descent into lower fidelity for timescales of multiple milliseconds. Even when evolving with the NV center in  $|m_s = 0\rangle$ , the presence of the (very fast) Larmor oscillation causes even small disturbances from slower, internuclear interactions to propagate and grow.

## 6.2. Pulse sequence 2: 12 orientations

Many-pulse sequences like A-24 may not be desirable to work with and are generally not preferable to sequences which have less pulses (that is, if performance is comparable). Therefore we might wish to restrict our ‘domain’ of orientations. One possible choice for such a restricted domain is table 5.2 with the entries corresponding to z-pulses over  $\pm\frac{\pi}{2}$  removed. This choice is somewhat arbitrary but it is important to remove entries along with the entire group to which they belong. One reason for preference towards removing rows in the table instead of columns would be that the rows correspond to effective rotations around the z-axis which are implemented in several concatenated multi-axis rotations, whereas the columns correspond to single pulses around x and y.

Optimizing for the described orientations yielded the following optimal evolution times:

$$\boldsymbol{\tau} = \frac{1}{12} \begin{bmatrix} 1 \\ 1 \\ 1 \\ \vdots \\ 1 \\ 1 \\ 1 \end{bmatrix}. \quad (6.3)$$

After the previous result this distribution of times is hardly surprising. We will name this sequence A-12 for easy reference. The following was obtained in terms of actual pulses:

$$-\tau - \left[\frac{\pi}{2}\right]_x - \tau - \left[-\frac{\pi}{2}\right]_x \left[\frac{\pi}{2}\right]_y - \tau - [\pi]_y - \tau - \left[\frac{\pi}{2}\right]_y \left[-\frac{\pi}{2}\right]_x - \tau - \left[-\frac{\pi}{2}\right]_x - \tau - [\pi]_y$$

$$-\tau - \left[-\frac{\pi}{2}\right]_x - \tau - \left[\frac{\pi}{2}\right]_x \left[-\frac{\pi}{2}\right]_y - \tau - [\pi]_y - \tau - \left[-\frac{\pi}{2}\right]_y \left[\frac{\pi}{2}\right]_x - \tau - \left[\frac{\pi}{2}\right]_x - \tau - [\pi]_y$$

Each  $\tau$  represents free evolution with a duration of 1/12 the total evolution time. Fidelity for total evolution times between 0-1 ms is shown below:

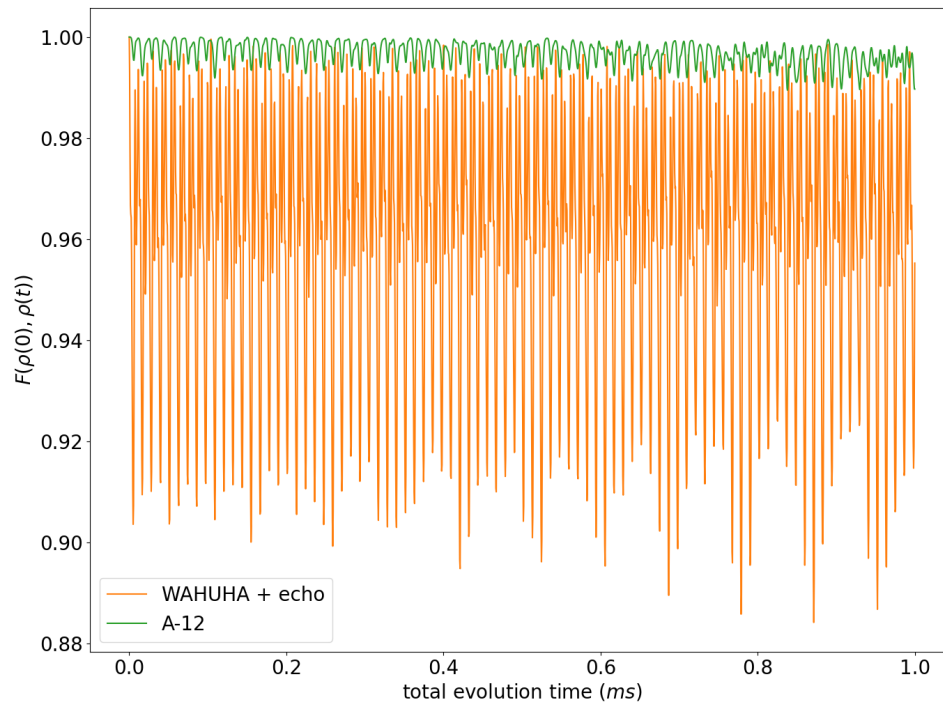


Figure 6.6: Fidelity for A-12 and WAHUHA + echo pulse sequences for total evolution time 1 ms. NV center was fixed in  $|m_s = -1\rangle$  state.

Comparing to 6.2 we see performance in terms of fidelity drop-off is very similar. One main difference lies in the slightly higher oscillation frequency which is present in the fidelity for A-24. This suggests A-12 might be somewhat less effective in cancelling the corresponding interactions.

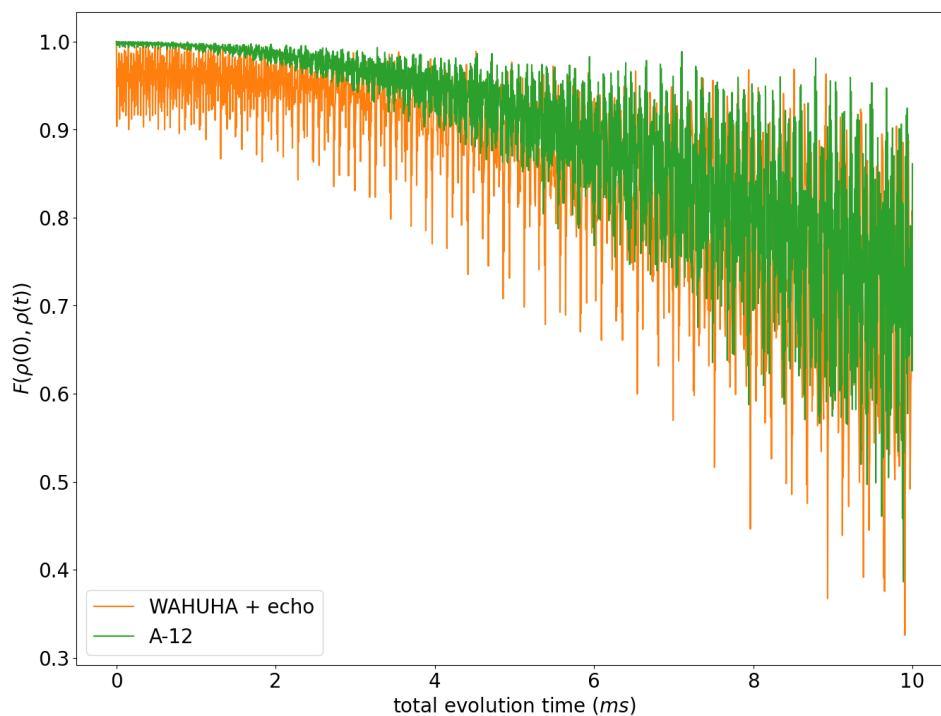


Figure 6.7: Fidelity for A-12 and WAHUHA + echo pulse sequences for total evolution time 10 ms. NV center was fixed in  $|m_s = -1\rangle$  state.

Again, the performance of the sequence deteriorates over the course of 10 ms.  
For the  $|m_s = 0\rangle$  state, a similar result to A-24 was obtained:

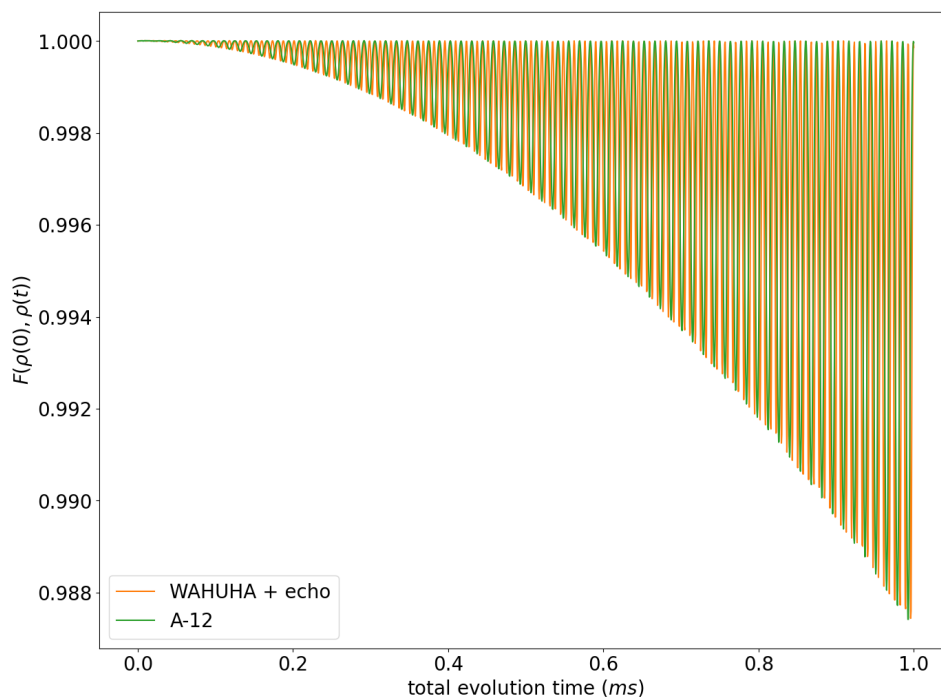


Figure 6.8: Fidelity for A-12 and WAHUHA + echo pulse sequences for total evolution time 1 ms. NV center was fixed in  $|m_s = 0\rangle$  state.

Again, we see a slow oscillation caused by internuclear interactions modulated with a harmonic of the Larmor frequency. As expected, the fast oscillation in fidelity for A-12 now has a frequency of  $1/6$  the Larmor frequency as compared to  $1/3$  the Larmor frequency for WAHUHA + echo, corresponding to A-12 having twice the number of evolution periods.

A note is that the frequencies of oscillations in fidelity do not necessarily correspond exactly to the coupling tables in the appendix. This is caused by the fact that the actual frequency of many-body interactions depends non-linearly on (differences between) coupling strengths.

Furthermore, the performance above was calculated assuming ideal pulses which do not have angle or axis errors and are instantaneous. This is, however, not realistic. The robustness of the designed pulse sequences to such errors will be the subject of discussion in the next chapter. WAHUHA + echo has been proven robust [21], so any errors incurred by the A-sequences may nullify the performance gain of these sequences over the first one. This will be among the subjects of discussion in the next chapter.

# 7

## Discussion

### 7.1. Consecutiveness of pulses

In this thesis, a linear programming framework was defined for optimizing evolution times in the context of first order AHT. However, arguably more effort was placed in determining the order of the evolution periods in each orientation, and the concatenation of these orientations by means of actual pulses. One might ask why an effort was undertaken to optimize for these orientations, instead of optimizing for series of pulses:

$$U_k = P_m P_{m-1} \cdots P_2 P_1, \quad (7.1)$$

where each  $P_i$  is one of the allowed (x- or y-) pulses. This is the approach which was followed in the original paper by O’Keeffe et al [5]. But this results in a number of difficulties. First of all, the pulses have to be consecutive:

$$\begin{aligned} U_0 &= I \\ U_1 &= P_1 \\ U_2 &= P_2 P_1 \\ &\vdots \\ U_m &= P_m P_{m-1} \cdots P_2 P_1. \end{aligned} \quad (7.2)$$

So per linear program, we can only optimize for the evolution times of a set sequence of pulses. Of course, we can do this for every possible pulse sequence of a given length. But even if we are using only x- and y-pulses over  $\pi$  or  $\pm\frac{\pi}{2}$  each, which gives us six possible pulses, we end up with a large number of variables. Even a comparatively modest 10-pulse sequence<sup>1</sup> would give a less modest  $6^{10} \approx 10^7$  possible pulse sequences. Also, some sort of symmetry selection has to be incorporated in the process because first-order AHT may not be accurate in its calculated Hamiltonians, especially over long evolution times. This could be optimized for automatically: higher order AHT terms could be calculated for each set of pulses and optimal pulse lengths after which resemblance to the zero matrix could be quantified, or the system could be propagated for different evolution times like in the previous chapter. But this adds to the computational load. Of course, if such a design pipeline were set up with sufficient computing power at its disposal, this would be very useful indeed. However, this is out of the scope of this thesis. Therefore a greater emphasis was placed behind the theory of pulse sequence design and the symmetry that goes with it.

### 7.2. Heterogeneous pulse combinations

One of the more interesting additions to the pulse design process as described in this thesis is the addition of heterogeneous pulses, i.e. not applying the same pulse to all qubits at once. Combined with an accurate characterization of the system at hand, this could utilize the LP framework in a very powerful way: a pulse sequence could be engineered which is tailored to specific system dynamics. Again, the drawback is the

<sup>1</sup>Of course, there exist many pulse sequences which are shorter than 10 pulses, such as the well-known WAHUA + echo sequence. However, with sequences as large as 48 pulses [21] a 10-pulse sequence would not be considered large.

number of variables. The number of possible AHT terms would scale as  $24^n$ , which grows impractically large after only a few qubits.

Moreover, tailoring (a set of) pulse combinations requires extremely detailed knowledge about a system with regards to the couplings which are present. In some applications, such knowledge might not be easily obtainable and therefore system non-specific globally applied pulse sequences are preferable.

### 7.3. Non-ideality of pulses

Perhaps the greatest influencing factor on the real-world performance of the designed pulse sequence is the non-ideality of pulse rotations. More specifically, inaccuracies in pulse application times can cause slight under- or overrotations. Choi et al. [21] proposed a framework for analysing robustness to such errors. This method is based on a notion of ‘chirality’ of the rotation. In fact this is nothing more than counting the sum of all rotations over the axes. For robustness to rotation angle errors, the requirement is that this sum is zero for each axis. In other words, this means we have rotated as much in the positive direction as in the negative direction for each of the x-, y-, and z-axis separately.

Using this representation it was determined that both A-24 and A-12 have non-zero chirality sums, corrupting the robustness of the A-sequences.

One reason for this is the bias toward positive rotations: all rotations over  $\pi$  use positive angles. This stems from the ideal pulse perspective: if pulses are instantaneous, a rotation over  $\pi$  over a certain axis is exactly the same as a rotation over  $-\pi$  over that same axis. But if pulses have actual duration, these two manners of rotating correspond to pulses in opposite directions, which has consequences for the amount of axis error. Furthermore, composite rotations (i.e. rotations around x- and y-axes directly after each other) can often be implemented in several ways. Using these tools, the A-sequences can be re-engineered to incorporate symmetry in the actual pulses which are applied as well. For example, this yields the following adaptation for A-12:

$$\begin{aligned} &-\tau - \left[\frac{\pi}{2}\right]_x - \tau - \left[-\frac{\pi}{2}\right]_x \left[\frac{\pi}{2}\right]_y - \tau - [\pi]_y - \tau - \left[\frac{\pi}{2}\right]_y \left[-\frac{\pi}{2}\right]_x - \tau - \left[-\frac{\pi}{2}\right]_x - \tau - [\pi]_y \\ &-\tau - \left[-\frac{\pi}{2}\right]_x - \tau - \left[\frac{\pi}{2}\right]_x \left[-\frac{\pi}{2}\right]_y - \tau - [-\pi]_y - \tau - \left[-\frac{\pi}{2}\right]_y \left[\frac{\pi}{2}\right]_x - \tau - \left[\frac{\pi}{2}\right]_x - \tau - [-\pi]_y \end{aligned}$$

The above sequence, which is equivalent to the sequence given in the Results section in terms of the orientations it ‘visits’, does give chirality sum 0. The same can be done for A-24 but this requires additional rotations, rendering the pulse sequence more difficult to implement. A better approach for A-24 would therefore be to re-order the orientations, taking symmetry into account, to arrive at a shorter sequence which is more easily corrected for chirality.

### 7.4. Tilted axis pulses

In this thesis, only pulses around the x- and y-axes were used to construct the pulse sequences. However, we could just as well tilt the rotation angle to any axis in the x-y plane. This could mean a more efficient (i.e. shorter) pulse sequence and remove the need for composite pulses. For example, rotating around the axis defined by  $\frac{1}{\sqrt{2}}\hat{x} + \frac{1}{\sqrt{2}}\hat{y}$  by  $\pi$  is the same as the composite of a  $\pi$  rotation around the x-axis and a  $\frac{\pi}{2}$  rotation around the y-axis. In fact, the rotation operator can be defined more generally than in equation 2.35:

$$R_j(\theta) = e^{-\frac{\theta}{2}\hat{n}\cdot\sigma}. \quad (7.3)$$

where  $\hat{n}$  is a unit vector in the direction of the axis of rotation and  $\sigma$  contains the three Pauli matrices.

The addition of such pulses to the AHT/linear programming framework could be readily implemented using the formula above. However, effects of tilted-axis rotation on the degree of pulse imperfection is yet to be determined. A similar method as in the above paragraph might be utilized, also counting the total effective rotation about the offset axes.

### 7.5. Coupling strengths

The coupling strengths of the 5-qubit system which was used are provided in the appendix. It immediately stands out that some NV-couplings are zero. This does not necessarily correspond to literature [23]. This is an artefact of the simulation method. First, the lattice was populated with lattice vectors and carbon spin positions were calculated from these. Then, relative position vectors between the carbon spins and NV center were calculated in order to compute interactions. But the same axis system was used in calculating the

---

interactions and in populating the lattice. Since the positions which can be occupied are discretized, it may very well happen that two lattice constituents share an x-, y- or z-coordinate. If this is the case, the dipolar interactions in that direction will be zero.



# 8

## Conclusion

In this thesis, a framework was set up for the design of NMR pulse sequences applied to a nitrogen-vacancy (NV) center in diamond. The NV center is a point defect in diamond which is used to form a qubit in a subspace between the  $m_s \in -1, 0$  states of the two unpaired electrons in its orbitals. Manipulation of this qubit is possible using microwave radiation. Because of strong dipolar interactions between the NV center and spin- $\frac{1}{2}$  carbon-13 nuclei, the NV center in diamond provides a useful environment for readout and control of carbon-13 spins.

The diamond structure was simulated in Python by randomly populating a grid with carbon-13 nuclei according to the natural occurrence percentage of carbon-13 and the crystal structure of diamond. The nitrogen vacancy center was placed in the middle of the simulation environment and dipolar couplings were calculated between the NV center and the carbon spins, as well as among the carbon spins (internuclear interactions).

The principles of Average Hamiltonian Theory (AHT) were discussed. AHT entails a technique for calculating the time-independent effective Hamiltonian over a time period in which a system is evolved according to a time-dependent Hamiltonian. Specifically, this theory was applied to the manipulation of a quantum system by the application of rotating pulses, followed by evolution periods of predetermined times. These pulses can be physically implemented by means of Rabi oscillations, i.e. rotating (the expectation values of) a spin through the application of static and rotating magnetic fields. Using such a scheme, an effective Hamiltonian over the total evolution period can be engineered by adjusting the types of pulses, the order in which they are applied and/or the durations of free evolution. An effective Hamiltonian which is identically zero was selected as a target, as this signifies complete decoupling of the system.

24 different Hamiltonian 'orientations' were defined corresponding to the 24 rotational symmetries of the cube. Due to cancellation of terms in AHT when the system Hamiltonian is (anti)symmetric in time, temporal symmetry of orientations was taken into account as a guiding principle in the pulse design. Evolution time for each of (a subset of) these orientations was then optimized for using linear programming implemented in Python. This was done by calculating the first-order AHT term corresponding to each orientation and projecting onto a vector. Optimizing for all possible orientations yielded pulse sequence A-24:

$$\begin{aligned} &-\tau - \left[\frac{\pi}{2}\right]_x - \tau - \left[-\frac{\pi}{2}\right]_x \left[\frac{\pi}{2}\right]_y - \tau - [\pi]_y - \tau - \left[\frac{\pi}{2}\right]_y \left[-\frac{\pi}{2}\right]_x - \tau - \left[-\frac{\pi}{2}\right]_x - \tau - \left[\frac{\pi}{2}\right]_x \left[-\frac{\pi}{2}\right]_y \left[\frac{\pi}{2}\right]_x - \tau - \left[-\frac{\pi}{2}\right]_y - \tau - \left[\frac{\pi}{2}\right]_y \left[\frac{\pi}{2}\right]_x \\ &-\tau - [\pi]_x - \tau - \left[\frac{\pi}{2}\right]_x \left[\frac{\pi}{2}\right]_y - \tau - \left[\frac{\pi}{2}\right]_y - \tau - [\pi]_x - \tau - \left[\frac{\pi}{2}\right]_y - \tau - \left[-\frac{\pi}{2}\right]_y \left[-\frac{\pi}{2}\right]_x - \tau - [\pi]_x - \tau - \left[-\frac{\pi}{2}\right]_x \left[-\frac{\pi}{2}\right]_y - \tau - \left[-\frac{\pi}{2}\right]_y \\ &-\tau - \left[\frac{\pi}{2}\right]_x \left[-\frac{\pi}{2}\right]_y \left[\frac{\pi}{2}\right]_x - \tau - \left[-\frac{\pi}{2}\right]_x - \tau - \left[\frac{\pi}{2}\right]_x \left[-\frac{\pi}{2}\right]_y - \tau - [\pi]_y - \tau - \left[-\frac{\pi}{2}\right]_y \left[\frac{\pi}{2}\right]_x - \tau - \left[\frac{\pi}{2}\right]_x - \tau - [\pi]_y \end{aligned}$$

where each evolution period corresponds to  $1/24$  of the total evolution time. The sequence of orientations was converted to an actual pulse sequence by means of a brute-force program. Performance was compared to the six-pulse WAHUHA + echo sequence [21] using density matrix fidelity as a function of total evolution time. Assuming perfect pulses, performance for this sequence (denoted as A-24) exceeded WAHUHA + echo for total evolution times below 5 ms and was comparable to WAHUHA + echo for larger timescales. Specifically, A-24 seemed more effective than WAHUHA + echo at removing high-frequency couplings caused by interactions between carbons and the NV center, as well as internuclear couplings.

Restricting the search space to 12 orientations yielded a shorter 12-pulse sequence A-12:

$$-\tau - \left[\frac{\pi}{2}\right]_x - \tau - \left[-\frac{\pi}{2}\right]_x \left[\frac{\pi}{2}\right]_y - \tau - [\pi]_y - \tau - \left[\frac{\pi}{2}\right]_y \left[-\frac{\pi}{2}\right]_x - \tau - \left[-\frac{\pi}{2}\right]_x - \tau - [\pi]_y$$

$$-\tau - \left[-\frac{\pi}{2}\right]_x - \tau - \left[\frac{\pi}{2}\right]_x \left[-\frac{\pi}{2}\right]_y - \tau - [-\pi]_y - \tau - \left[-\frac{\pi}{2}\right]_y \left[\frac{\pi}{2}\right]_x - \tau - \left[\frac{\pi}{2}\right]_x - \tau - [-\pi]_y$$

A motivation of this is the non-ideality of pulses, which limits the usefulness and accuracy of many-pulse sequences like A-24. The optimal evolution time for each of the orientations respectively was determined to be 1/12 of total duration. Performance of A-12 was similar to A-24 but the shorter sequence was slightly less effective at cancelling out higher frequency interactions.

The above performances were calculated assuming ideal pulses, which is not realistic. Using the method of chirality summation proposed by Choi et al. [21], the sequences A-12 and A-24 were calculated to be non-robust towards imperfections in pulse application. However, there are some degrees of freedom in the choice of pulses for rotating between orientations. As such, the sequences can be adapted to incorporate robustness into the design at a pulse level. For A-24 however, incorporating this robustness would mean introducing additional pulses. This is best avoided by re-ordering the orientations in a symmetrical way.

# A

## Tables of couplings

	$A_{zz}$ (Hz)	$A_{zy}$ (Hz)	$A_{zx}$ (Hz)
C1	154907,0	0,0	0,0
C2	77589,7	99758,2	0,0
C3	-49827,5	0,0	-15253,3
C4	31237,4	-3194,7	-9584,2
C5	-29811,9	29811,9	-29811,9

Table A.1: Couplings to NV center for the 5 used qubits in Hz.

	C1	C2	C3	C4	C5
C1	0,0	45,6	-12,2	15,8	0,0
C2	45,6	0,0	-8,5	5,1	-1,3
C3	-12,2	-8,5	0,0	-4,9	-2,3
C4	15,8	5,1	-4,9	0,0	0,1
C5	0,0	-1,3	-2,3	0,1	0,0

Table A.2: Internuclear couplings for the 5 used qubits in Hz.



# B

## Analytical result

$$\frac{1}{2}((\cos(\frac{t\omega_L}{3}) - 3)^2 \sin^2(\frac{tC_{zz}}{2}) \sin^4(\frac{t\omega_L}{6}) + \sin^2(\frac{tC_{zz}}{4}) \sin^2(\frac{t\omega_L}{3})(-4 \sin(\frac{t\omega_L}{6}) + \sin(\frac{tC_{zz}}{4}) + \sin(\frac{t\omega_L}{3}))^2) \quad (\text{B.1})$$

Note that this result was obtained by using the WAHUHA + echo sequence as provided in Choi et al., thus with the qubit ending in the  $| -x \rangle$  state.



# Bibliography

- [1] J. Randall et al. “Many-body localized discrete time crystal with a programmable spin-based quantum simulator”. In: *Science* 374.6574 (2021), pp. 1474–1478. DOI: 10.1126/science.abk0603. eprint: <https://www.science.org/doi/pdf/10.1126/science.abk0603>. URL: <https://www.science.org/doi/abs/10.1126/science.abk0603>.
- [2] Frank Wilczek. “Quantum time crystals”. In: *Physical review letters* 109.16 (2012), p. 160401.
- [3] Paul Adrien Maurice Dirac. “A new notation for quantum mechanics”. In: *Mathematical Proceedings of the Cambridge Philosophical Society*. Vol. 35. 3. Cambridge University Press, 1939, pp. 416–418.
- [4] David Jeffery Griffiths and Darrell F. Schroeter. “12.3”. In: *Introduction to quantum mechanics*. 3rd ed. Cambridge University Press, 2018, pp. 455–459.
- [5] Michael F O’Keeffe et al. “Hamiltonian engineering with constrained optimization for quantum sensing and control”. In: *New Journal of Physics* 21.2 (2019), p. 023015.
- [6] Oliveira Iván S. “2.6 NMR of noninteracting spins  $1/2$ ”. In: *NMR Quantum Information Processing*. Elsevier, 2007, pp. 47–48.
- [7] Oliveira Iván S. “2.3 Interaction with a radiofrequency field - the resonance phenomenon”. In: *NMR Quantum Information Processing*. Elsevier, 2007, pp. 38–41.
- [8] Michael A. Nielsen and Isaac L. Chuang. “9 Distance measures for quantum information”. In: *Quantum Computation and Quantum Information*. Cambridge University Press, 2021, pp. 409–410.
- [9] *5: The precession of a top spinning in the gravitational field ...* URL: [https://www.researchgate.net/figure/The-precession-of-a-top-spinning-in-the-gravitational-field-analogous-to-the-nuclear\\_fig4\\_333130675](https://www.researchgate.net/figure/The-precession-of-a-top-spinning-in-the-gravitational-field-analogous-to-the-nuclear_fig4_333130675).
- [10] Oliveira Iván S. “2.2 Interaction with static magnetic fields”. In: *NMR Quantum Information Processing*. Elsevier, 2007, pp. 35–37.
- [11] David Jeffery Griffiths and Darrell F. Schroeter. “11”. In: *Introduction to quantum mechanics*. 3rd ed. Cambridge University Press, 2018, pp. 402–413.
- [12] H. Holloway et al. “Isotopic dependence of the lattice constant of diamond”. In: *Phys. Rev. B* 44 (13 Oct. 1991), pp. 7123–7126. DOI: 10.1103/PhysRevB.44.7123. URL: <https://link.aps.org/doi/10.1103/PhysRevB.44.7123>.
- [13] *Diamond NV Center magnetometry*. Oct. 2020. URL: <https://www.nist.gov/programs-projects/diamond-nv-center-magnetometry>.
- [14] CE Bradley. “Order from Disorder: Control of Multi-Qubit Spin Registers in Diamond”. In: (2021), pp. 12–15.
- [15] Bas Hensen. “Quantum Nonlocality with Spins in Diamond”. English. PhD thesis. Delft University of Technology, Apr. 2016. ISBN: 978-90-8593-253-6. DOI: 10.4233/uuid:b307dca0-79a4-4cc9-af91-a2927a61088e.
- [16] M. W. Doherty et al. “Theory of the ground-state spin of the  $NV^-$  center in diamond”. In: *Phys. Rev. B* 85 (20 May 2012), p. 205203. DOI: 10.1103/PhysRevB.85.205203. URL: <https://link.aps.org/doi/10.1103/PhysRevB.85.205203>.
- [17] Oliveira Iván S. “2.7 Nuclear spin interactions”. In: *NMR Quantum Information Processing*. Elsevier, 2007, pp. 52–61.
- [18] Nan Zhao, Sai-Wah Ho, and Ren-Bao Liu. “Decoherence and dynamical decoupling control of nitrogen vacancy center electron spins in nuclear spin baths”. In: *Physical Review B* 85.11 (2012), p. 115303.
- [19] Andreas Brinkmann. “Introduction to average Hamiltonian theory. I. Basics”. In: *Concepts in Magnetic Resonance Part A* 45.6 (2016), pp. 6–7.

- 
- [20] Sergio Blanes et al. “The Magnus expansion and some of its applications”. In: *Physics reports* 470.5-6 (2009), pp. 151–238.
- [21] Joonhee Choi et al. “Robust dynamic hamiltonian engineering of many-body spin systems”. In: *Physical Review X* 10.3 (2020), p. 031002.
- [22] Malcolm H Levitt. “Symmetry in the design of NMR multiple-pulse sequences”. In: *The Journal of chemical physics* 128.5 (2008), p. 052205.
- [23] MH Aboeih et al. “Atomic-scale imaging of a 27-nuclear-spin cluster using a quantum sensor”. In: *Nature* 576.7787 (2019), pp. 411–415.